NASA/TM–2010-216404

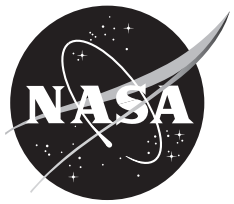

Boeing-SMART Rotor Wind Tunnel Test Data Report for DARPA Helicopter Quieting Program (HQP) Phase 1B

Benton H. Lau, Nicole Obriecht, Tanner Gasow, Brandon Hagerty, and Kelly C. Cheng
Ames Research Center, Moffett Field, California

Ben W. Sim
U.S. Army Aeroflightdynamics Directorate
Ames Research Center, Moffett Field, California

September 2010

Report Documentation Page

Form Approved
OMB No. 0704-0188

1. REPORT DATE	2. REPORT TYPE	3. DATES COVERED
SEP 2010		**00-00-2010 to 00-00-2010**

4. TITLE AND SUBTITLE	5a. CONTRACT NUMBER
Boeing-SMART Rotor Wind Tunnel Test Data Report for DARPA Helicopter Quieting Program (HQP) Phase 1B	5b. GRANT NUMBER
	5c. PROGRAM ELEMENT NUMBER
6. AUTHOR(S)	5d. PROJECT NUMBER
	5e. TASK NUMBER
	5f. WORK UNIT NUMBER
7. PERFORMING ORGANIZATION NAME(S) AND ADDRESS(ES) **U.S. Army Aeroflightdynamics Directorate,Ames Research Center,Moffett Field,CA,94035**	8. PERFORMING ORGANIZATION REPORT NUMBER
9. SPONSORING/MONITORING AGENCY NAME(S) AND ADDRESS(ES)	10. SPONSOR/MONITOR'S ACRONYM(S)
	11. SPONSOR/MONITOR'S REPORT NUMBER(S)

12. DISTRIBUTION/AVAILABILITY STATEMENT
Approved for public release; distribution unlimited

13. SUPPLEMENTARY NOTES

14. ABSTRACT

15. SUBJECT TERMS

16. SECURITY CLASSIFICATION OF:			17. LIMITATION OF ABSTRACT	18. NUMBER OF PAGES	19a. NAME OF RESPONSIBLE PERSON
a. REPORT	b. ABSTRACT	c. THIS PAGE			
unclassified	**unclassified**	**unclassified**	**Same as Report (SAR)**	**68**	

The NASA STI Program Office . . . in Profile

Since its founding, NASA has been dedicated to the advancement of aeronautics and space science. The NASA Scientific and Technical Information (STI) Program Office plays a key part in helping NASA maintain this important role.

The NASA STI Program Office is operated by Langley Research Center, the Lead Center for NASA's scientific and technical information. The NASA STI Program Office provides access to the NASA STI Database, the largest collection of aeronautical and space science STI in the world. The Program Office is also NASA's institutional mechanism for disseminating the results of its research and development activities. These results are published by NASA in the NASA STI Report Series, which includes the following report types:

- TECHNICAL PUBLICATION. Reports of completed research or a major significant phase of research that present the results of NASA programs and include extensive data or theoretical analysis. Includes compilations of significant scientific and technical data and information deemed to be of continuing reference value. NASA's counterpart of peer-reviewed formal professional papers but has less stringent limitations on manuscript length and extent of graphic presentations.

- TECHNICAL MEMORANDUM. Scientific and technical findings that are preliminary or of specialized interest, e.g., quick release reports, working papers, and bibliographies that contain minimal annotation. Does not contain extensive analysis.

- CONTRACTOR REPORT. Scientific and technical findings by NASA-sponsored contractors and grantees.

- CONFERENCE PUBLICATION. Collected papers from scientific and technical conferences, symposia, seminars, or other meetings sponsored or cosponsored by NASA.

- SPECIAL PUBLICATION. Scientific, technical, or historical information from NASA programs, projects, and missions, often concerned with subjects having substantial public interest.

- TECHNICAL TRANSLATION. English-language translations of foreign scientific and technical material pertinent to NASA's mission.

Specialized services that complement the STI Program Office's diverse offerings include creating custom thesauri, building customized databases, organizing and publishing research results . . . even providing videos.

For more information about the NASA STI Program Office, see the following:

- Access the NASA STI Program Home Page at *http://www.sti.nasa.gov*

- E-mail your question via the Internet to help@sti.nasa.gov

- Fax your question to the NASA Access Help Desk at (301) 621-0134

- Telephone the NASA Access Help Desk at (301) 621-0390

- Write to:
  NASA Access Help Desk
  NASA Center for AeroSpace Information
  7115 Standard Drive
  Hanover, MD 21076-1320

NASA/TM–2010-216404

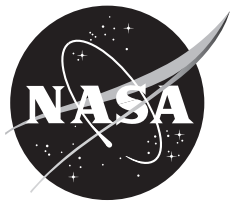

Boeing-SMART Rotor Wind Tunnel Test Data Report for DARPA Helicopter Quieting Program (HQP) Phase 1B

Benton H. Lau, Nicole Obriecht, Tanner Gasow, Brandon Hagerty, and Kelly C. Cheng
Ames Research Center, Moffett Field, California

Ben W. Sim
U.S. Army Aeroflightdynamics Directorate
Ames Research Center, Moffett Field, California

National Aeronautics and
Space Administration

Ames Research Center
Moffett Field, California 94035-1000

September 2010

Acknowledgments

The SMART wind tunnel test was funded by the Helicopter Quieting Program of DARPA and the NASA Subsonic Rotary-Wing Program. The authors would like to acknowledge valuable contributions from many dedicated staffs at Boeing, DARPA, NASA, NFAC, Army, MIT, UCLA, and the University of Maryland. In particular, the authors would like to thank Dr. Friedrich Straub (Boeing) as the Principal Investigator of the Boeing-SMART program for the helpful discussion, Mr. Randall Peterson at NASA Ames for data post-processing and RDMS support, and Dr. Daniel Newman (DARPA), Mr. Thomas Maier (AFDD), Ms. Susan Gorton (NASA), and Dr. Wayne Johnson and Dr. William Warmbrodt (NASA Ames) for their support on the test.

Table of Contents

List of Figures

List of Figures (cont.)

List of Tables

Nomenclature List

A	Rotor disk area, πR^2, ft^2
C_T	Rotor thrust coefficient, parallel to the rotor shaft, $T/\rho A(\Omega R)^2$
C_P	Rotor power coefficient, $P/\rho A(\Omega R)^3$
M_{adv}	Advancing tip Mach number, $(V+\Omega R)/a$
M_{tip}	Hover tip Mach number, $\Omega R/a$
P	Rotor power, Hp
R	Rotor radius, 16.925 ft
S_R	Blade reference area, 67.49 ft^2
T	Rotor thrust, lbf
V	Wind tunnel speed, ft/s
a	Speed of sound, ft/s
c	Blade constant section chord, 10 in.
c_f	Active flap chord, $0.35c$
r, ψ, θ	Spherical coordinate system, $+r$ radially out (ft), $+\psi$ azimuthal angle (deg), $+\theta$ above reference plane (deg)
t	Airfoil thickness
x, y, z	Cartesian coordinate system, $+x$ downstream, $+y$ starboard, $+z$ up, ft
Ω	Rotor rotational speed, rpm
α_{su}, α_{sc}	Uncorrected and corrected shaft angle of attack, positive tilting back, deg
β, ϕ	Harmonic amplitude and phase of active flap deflection, deg
δ	Active flap deflection, positive down, deg
μ	Advance ratio, $V/(\Omega R)$
ψ	Blade azimuth angle, positive counterclockwise with zero at downstream, deg
ρ	Air density, slug/ft^2
σ	Rotor solidity, $S_R/\pi R^2$, 0.075

Subscript List

a	Coordinate system reference to advancing blade tip
h	Coordinate system reference to hub center
k	Blade number index, 1 to 5
n	Harmonic index (0 to *N*) or harmonic frequency (per rev)
boe	Boeing convention
rdms	NASA/RDMS convention

BOEING-SMART ROTOR WIND TUNNEL TEST DATA FOR DARPA HELICOPTER QUIETING PROGRAM (HQP) PHASE 1B

Benton H. Lau,[1] Nicole Obriecht,[1] Tanner Gasow, [1] Brandon Hagerty, [1]
Kelly C. Cheng,[1] and Ben W. Sim[2]

Ames Research Center

Introduction

The Tactical Technology Office of the Defense Advanced Research Projects Agency (DARPA) initiated the Helicopter Quieting Program (HQP) in 2004 to develop high fidelity, state-of-the-art computational tools for designing advanced helicopter rotors with reduced acoustic perceptibility and enhanced performance. A critical step towards this achievement is the development of rotorcraft prediction codes capable of assessing a wide range of helicopter configurations and operations for future rotorcraft designs. This includes novel next-generation rotor systems that incorporate innovative passive and/or active elements to meet future challenging military performance and survivability goals.

Phase I of the HQP program involved development of prediction methodologies ("tools") by coupling computational structural dynamics (CSD) to computational fluid dynamics (CFD) modeling codes. Participants included Stanford University/University of Maryland (SM), Georgia Institute of Technology/Pennsylvania State University (GP) and Teledyne Sciences Corporation. Phase I was primarily geared towards validating these prediction tools for conventional rotors currently in use by the fleet. Results from the participants demonstrated significant improvements in prediction accuracy and correlations (ref. 1) over classical comprehensive methods in all aspects of aerodynamics, structural, and acoustics responses of the rotor.

Phase Ib, with participants from SM and GP, was initiated in 2007 to demonstrate the robustness of HQP tools in the characteristics of *unconventional* rotor designs that utilize innovative on-blade active controls for dynamic tuning. An active flap rotor currently under development at Boeing (i.e., the Boeing-SMART rotor) was selected as the candidate for this code validation effort. Participants were asked to make blind predictions prior to full-scale rotor testing in the 40- by 80-Foot Wind Tunnel of the National Full-Scale Aerodynamics Complex (NFAC) at NASA Ames Research Center. This report details *experimental data* acquired from the SMART test and presents the acquired data in HQP-specific formats to enable correlations/comparisons with participants' predictions.

[1] Aeromechanics Branch, Ames Research Center, Moffett Field, CA 94035-1000.
[2] U.S. Army Aeroflightdynamics Directorate, Ames Research Center, Moffett Field, CA 94035-1000.

HQP Phase Ib Test Conditions

Table 1 lists the five flight cases prescribed by DARPA/HQP for the Phase Ib code validation effort with the Boeing-SMART rotor. Test conditions include low-to-high rotor speeds and descending flight configurations with and without active-flap operations. These test conditions offer variations in shaft angle, thrust, wind speed, and trailing-edge flap settings. Following Boeing's definition, the active flap deflection angle (δ_k) resulting from a commanded flap schedule of harmonic magnitude (β_n)/frequency (n)/phase ($\phi_{n\ boe}$) combination is expressed as $\delta_k(\psi_k) = \Sigma_n\ \beta_n \cdot \sin(n \cdot \psi_k + \phi_{n\ boe})$. Cases designated with SMART in the header pertain to conditions with active-flap excitations. The MDART case refers to a no-flap excitation case (i.e., 0° flap deflection) to simulate a base-line condition (ref. 2). For each of the selected test cases, DARPA required data from three in-plane microphones, rotor performance, control inputs, and blade structural loads (ref. 3).

Boeing-SMART Rotor Hardware

The SMART rotor test in the NFAC wind tunnel was a joint effort by DARPA, NASA, Army, and Boeing, with participations from the University of California at Los Angeles, Massachusetts Institute of Technology, and the University of Maryland. A modified full-scale MD 902 Explorer rotor with on-blade piezoelectric-actuated trailing-edge flap was used to demonstrate the capabilities of active-flap technology in forward flight.

The five-bladed bearingless rotor has an HH-10 (12% thick) airfoil at the inboard section and an HH-06 (9.5% thick) airfoil at the outboard section. The blade region from 0.93R to the tip has a parabolic leading-edge sweep (22° at the tip) with straight trailing edge and a 2:1 taper ratio. Table 2(a) lists a summary of the SMART rotor characteristics (refs. 4,5).

The active flap, which spanned radially between 0.74R to 0.92R, has a 25% chord with the piezoelectric actuators embedded in the blade spar at 0.74R (fig. 1). The actuators are designed to drive the trailing-edge flap at frequencies from two-per-rev (2P) up to six-per-rev (6P) with as much as a 6° amplitude. A continuous-time higher harmonic controller (CTHHC) developed by Hall et al. (ref. 6) was used to individually command the desired active flap angle of each blade (ref. 5). Table 2(b) summarizes the active-flap characteristics.

TABLE 1. PRESCRIBED FLIGHT CONDITIONS FOR DARPA HQP PHASE IB

Case	C_T/σ	α_{sc}	μ	M_{adv}	Flap schedule
MDART	0.080	-9.1°	0.300	0.805	$\delta_k=0°$
SMART 1	0.080	-9.1°	0.300	0.805	$\delta_k=2°\cdot\sin(5\cdot\psi_k+90°)$
SMART 2	0.080	-9.1°	0.300	0.805	$\delta_k=2°\cdot\sin(3\cdot\psi_k+60°)$
SMART 3	0.070	-9.1°	0.375	0.852	$\delta_k=1°\cdot\sin(5\cdot\psi_k+180°)$
SMART 4	0.075	+1.5°	0.200	0.746	$\delta_k=2°\cdot\sin(2\cdot\psi_k+240°)+1°\cdot\sin(5\cdot\psi_k+330°)$

k = blade index 1 to 5

Test Setup

The 11-week-long test in the NFAC wind tunnel began in February of 2008. The SMART rotor was installed on Boeing's Large Rotor Test Stand (LRTS) with the rotor hub 23.8 ft above the acoustic lining of the tunnel floor. The LRTS was supported by two main front-struts and a telescoping tail-strut. Tail-strut retraction provided positive, uncorrected shaft angle of attack (α_{su}) for the LRTS. Connected by a vertical test-stand strut, the LRTS consisted of an upper and a lower housing. The upper housing enclosed the rotor balance and hydraulic servo-actuators for the rotor control system while the lower housing enclosed a 1,500-HP General Electric motor and its transmission. A five-component rotor balance was mounted on top of a static mast that connected to the rotor hub in the upper housing. The balance measured three forces (lift, drag, and side) and two moments (pitch and roll). Torque was passed directly to the rotor hub through the rotating drive shaft that was confined in the static mast. Rotor torque was measured on the flex coupling between the drive shaft and the rotor. Figure 2 shows the model installation in the NFAC wind tunnel.

TABLE 2. BOEING-SMART CHARACTERISTICS FOR (A) ROTOR AND (B) ACTIVE FLAP

(a) Rotor

Rotor	Modified MD 900
Hub type	Bearingless
Number of blades	5
Radius, ft	16.925
Blade chord, in.	10
Airfoil	HH-10, t/c = 12%; $r/R < 0.74$
	HH-06, t/c = 9.5%; $r/R > 0.84$
Tip sweep	Parabolic leading-edge, $r/R > 0.93$; 22° at tip
Tip taper	2:1 straight trailing edge
Twist rate	–10°
Rotor solidity	0.075
Nominal rotor speed, rpm	392
Nominal tip speed, ft/s	695
Nominal thrust, lbf	5811
Nominal C_T/σ	0.075

(b) Active flap

Radial span	$0.739 \le r/R \le 0.916$
Chord, c_f	0.35c
Hinge location	0.75c
Control horn length, in.	0.75
Max flap angle	±6°
Flap weight, lbm	1.26

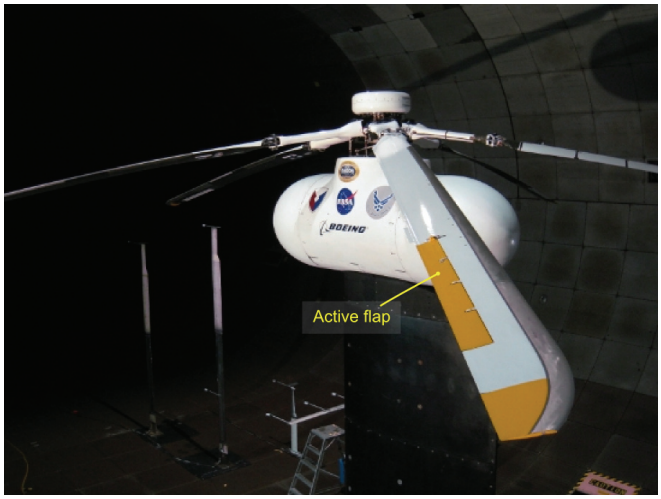

Figure 1. Boeing-SMART rotor with active trailing-edge flaps in the NFAC 40- by 80-Foot Wind Tunnel.

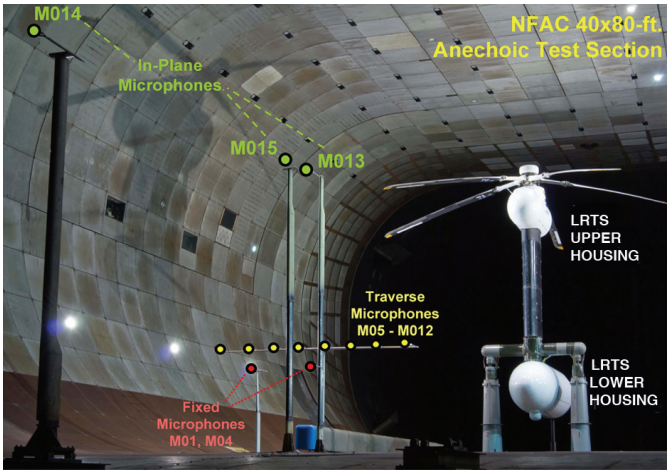

Figure 2. Boeing-SMART rotor mounted on the LRTS in the wind tunnel.

Instrumentation

During the Boeing-SMART rotor test, a set of microphones was strategically placed around the model to capture rotor noise sources of interest (fig. 2). These microphones were grouped into: a) out-of-plane fixed microphones (M1 and M4) to correlate to microphones used previously in the MDART test (ref. 2); b) traverse microphones (M5 through M12) that can be moved along guided rails for out-of-plane blade-vortex interaction noise mapping; and c) in-plane microphones (M13, M14, and M15) for low-frequency, in-plane rotor-noise measurement. Microphones M13, M14 and M15 were mounted on tower struts to be near in-plane of the rotor (approximately 10° below wind tunnel horizon). These microphones were also intentionally positioned along a straight line originating from the advancing blade tip to the tunnel centerline (fig. 3) to help determine near-field/far-field characteristics of in-plane rotor noise. With the exception of M14, all microphones were located within the

acoustically-treated portion of the 40- by 80-foot test section. Summaries of the microphone positions, relative to both the rotor hub center and the advancing blade tip (both at zero shaft tilt), are given in tables 3a and 3b respectively. To account for non-zero shaft tilt angle (α_{su}), the microphone coordinates must be transformed accordingly using the pivot point located 163 inches below the rotor hub.

In addition to the microphone and the rotor-balance measurements, other measurements included the rotating-blade channels, the stationary channels, and the wind tunnel channels. Since blade #1 was the primary blade, it was fully instrumented with rotating-blade channels including the flap, the lag, and the torsional strain gauges on the flex beam, the pitchcase, and the blade at various stations as shown in figure 4. During the test, the critical flap-bending gauge on the flex beam at station 9 at r/R=0.044 was used by the rotor operator to minimize blade flapping, and hence hub moments, at the desired test point (ref. 7). An active backup channel of the same strain gauge on blade #2 was also acquired. Other rotating channels included the active-flap position of each blade measured through the linear voltage differential transformer (LVDT) sensor, the input voltage, and current to the piezoelectric actuators. The stationary channels included the nonrotating swashplate positions, the rotor speed, the test-stand vibration, and the Interrange Instrumentation Group B (IRIG-B) time code. The wind tunnel channels included model shaft angle of attack, temperature, pressure, humidity, etc. related to the wind tunnel condition. Beside measurement channels, there are derived quantities, like air density, advance ratio, rotor collective, etc., which are calculated from multiple measurement channels. A complete list of measurement and derived channels presented in this report is summarized in Appendix A.

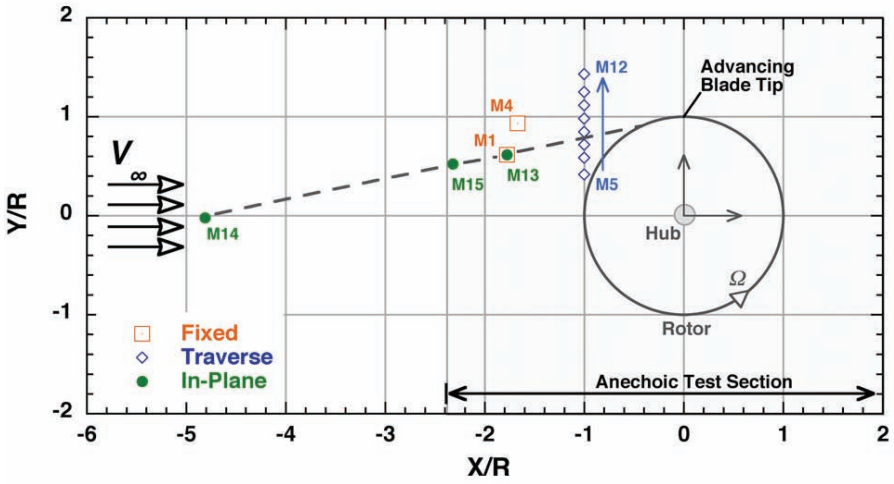

Figure 3. Top view of the test setup of the microphone layout with rotor hub at α_{su} = 0º.

TABLE 3A. HUB-CENTERED MICROPHONE POSITION AT α_{SU}= 0°

Mic. No.	x_h, ft	y_h, ft	z_h, ft	r_h, ft	r_h/R	ψ_h, deg	θ_h, deg	Notes
M1	-29.67	10.27	-17.94	36.16	2.14	160.9	-29.7	Fixed
M4	-27.92	15.59	-17.87	36.63	2.16	150.8	-29.2	Fixed
M5	16.73	6.97	-15.13	23.61	1.39	157.4	-39.9	Traverse
M6	-16.73	9.79	-15.13	24.59	1.45	149.7	-38.0	Traverse
M7	16.73	12.02	-15.13	25.56	1.51	144.3	-36.3	Traverse
M8	-16.73	14.17	-15.13	26.64	1.57	139.7	-34.6	Traverse
M9	-16.73	16.42	-15.13	27.90	1.65	135.5	-32.8	Traverse
M10	-16.73	18.67	-15.13	29.28	1.73	131.9	-31.1	Traverse
M11	-16.73	20.90	-15.13	30.75	1.82	128.7	-29.5	Traverse
M12	-16.73	23.92	-15.13	32.88	1.94	125.0	-27.4	Traverse
M13	**-29.67**	**10.27**	**-5.34**	**31.85**	**1.88**	**160.9**	**-9.7**	**In-plane**
M15	**-38.77**	**8.73**	**-7.13**	**40.38**	**2.39**	**167.3**	**-10.2**	**In-plane**
M14	**-80.38**	**-0.33**	**-14.84**	**81.72**	**4.83**	**180.2**	**-10.5**	**In-plane**

TABLE 3B. ADVANCING BLADE-TIP-CENTERED MICROPHONE POSITIONS AT α_{SU}= 0°

Mic. No.	x_a, ft	y_a, ft	z_a, ft	r_a, ft	r_a/R	ψ_a, deg	θ_h, deg	Notes
M1	-29.67	-6.43	-17.94	35.26	2.11	192.2	-30.6	Fixed
M4	-27.92	-1.11	-17.87	33.17	1.99	182.3	-32.6	Fixed
M5	-16.73	-9.73	-15.13	24.57	1.47	210.2	-38.0	Traverse
M6	-16.73	-6.91	-15.13	23.59	1.41	202.4	-39.9	Traverse
M7	-16.73	-4.68	-15.13	23.04	1.38	195.6	-41.1	Traverse
M8	-16.73	-2.53	-15.13	22.70	1.36	188.6	-41.8	Traverse
M9	-16.73	-0.28	-15.13	22.56	1.35	181.0	-42.1	Traverse
M10	-16.73	1.97	-15.13	22.64	1.36	173.3	-41.9	Traverse
M11	-16.73	4.20	-15.13	22.94	1.37	165.9	-41.3	Traverse
M12	-16.73	7.22	-15.13	23.68	1.42	156.7	-39.7	Traverse
M13	**-29.67**	**-6.43**	**-5.34**	**30.82**	**1.85**	**192.2**	**-10.0**	**In-plane**
M15	**-38.77**	**-7.97**	**-7.13**	**40.22**	**2.41**	**191.6**	**-10.2**	**In-plane**
M14	**-80.36**	**-17.03**	**-14.84**	**83.47**	**5.00**	**192.0**	**-10.2**	**In-plane**

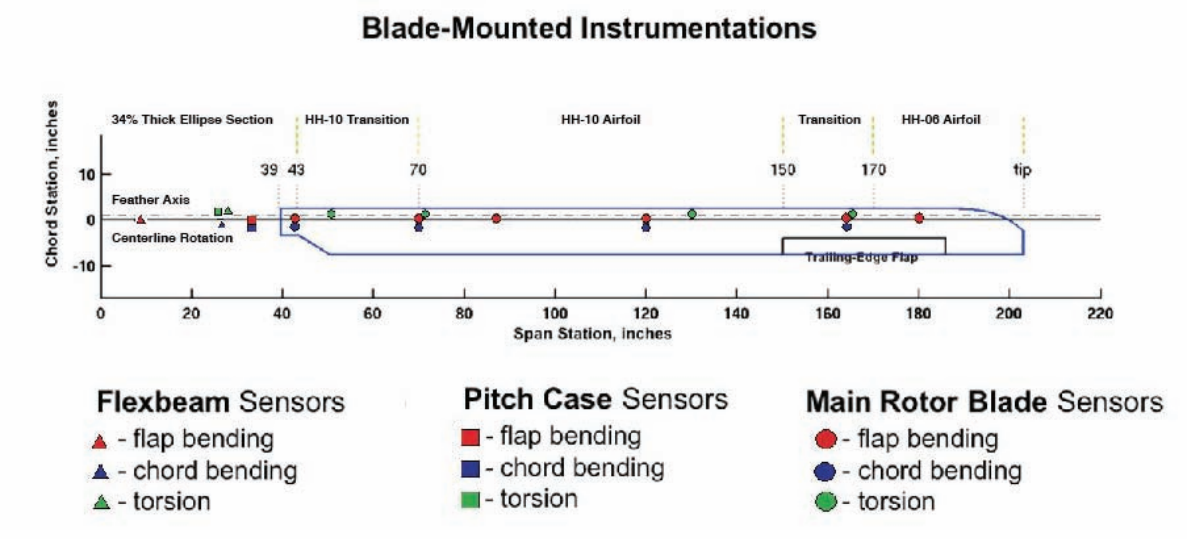

Figure 4. Position of strain gauges on blade #1 of the Boeing-SMART rotor.

Data Acquisition Systems and Post-Test Data Processing

The SMART test utilized two sets of data acquisition systems: the NFAC system and the Boeing system. The 12-bit Boeing data system consisted of a rotating and a stationary units. The stationary data unit mounted on top aft of the right main-strut was responsible for acquiring all stationary channels, the wind tunnel channels, a few fixed microphone channels, and a reference channel. The rotating data unit enclosed in a circular fairing on top of the rotor hub acquired all rotating channels and transmitted them through the slip rings. Both units provided signal conditioning to the sensors, and digitized and transmitted the data as pulse code modulation (PCM) streams at 10Mb/s. The PCM streams were then combined and recorded on a digital tape and a computer in the wind tunnel control room (ref. 8). The Boeing system acquired all data continuously at fixed sampling rates, mostly at 1250 Hz but some at 0.3333, 625, 3750, 10k, and 15k Hz.

Unlike the Boeing time-base data system, the NFAC data system acquired all data simultaneously at two rotor-synchronized rates: 256 samples/rev for wind tunnel channels and 2048 samples/rev for all (AC-coupled) microphone channels. For each test point, 64 revolutions of data (about 9.8s) were recorded. Synchronized azimuth-based sampling allows the extraction of exceptional signal-to-noise ratios associated with the rotational harmonics of the rotor. Any fluctuations not associated with the rotor harmonic frequencies are suppressed by the azimuth-based technique when averaged over all 64 revolutions of data. The high sampling rate with 24-bit resolution provides exceptional fidelity for acoustic data.

Post-test data processing for the Boeing data involves more steps than that for the NFAC data. The reference channel (a 0.2-Hz triangle waveform) was used as the time alignment reference between the Boeing and the NFAC data systems. Then 64 revolutions of Boeing data were extracted for processing and corrected for time shifting due to sequential sampling of the PCM systems and a 7º offset of the 1/rev encoder. The Boeing data were then

spline-fitted to 256 samples/rev and converted from raw counts into engineering units. Phase correction for the anti-aliasing filter was also applied and then stored on the Rotor Data Management System (RDMS) data server. Since NFAC data were sampled simultaneously and synchronously with the rotor speed, the only correction to the NFAC data was the 7º offset of the 1/rev encoder. After the Boeing and the NFAC data were merged together onto the RDMS server, the server applied tare corrections to the rotor balance data, calculated statistical values for all channels and harmonics, and computed different sound pressure calculations for microphone channels. For consistency, all rotor and wind tunnel channels in this report come from the Boeing data system while all microphone channels come from the NFAC data system. In accordance with HQP reporting guidelines, smooth time-history data are synthesized from the first 1024 harmonics for microphone channels and the first 10 harmonics for all other channels.

Data Repeatability and Selection

During the wind tunnel test, the high-speed SMART3 case experienced unexpected high vibratory hub and blade loads. No data was collected for that particular test case. In-situ testing, as well as information from the flex-beam manufacturer, identified some discrepancies in the flex-beams used in the Boeing-SMART test as compared to the 1992 MDART test (ref. 2). The high vibratory load issues encountered by the Boeing-SMART rotor were due to load limits based on previous MDART rotor properties from 1992. Preliminary investigations determined that the flex-beams on the Boeing-SMART rotor were approximately four times stiffer than that on the 1992 MDART rotor and the 2003 SMART rotor in the whirl-tower test (ref. 9). All other test cases were tested successfully.

Multiple test points were acquired for each of the four cases: MDART, SMART1, SMART2, and SMART4. It was necessary to select one representative data point per HQP test case to validate predictions. This process began by gathering all data points acquired for the test and categorizing them with the appropriate test case in a spreadsheet. The mean statistical data were downloaded from the RDMS data server and compared with the rotor/wind tunnel operating parameters that are known to govern acoustics radiation to the first order (ref. 10). Test-point selections were based on how close the mean operating conditions were to the desired HQP test conditions. Table 4 summarizes which data points remained after all the points were evaluated.

Once the data points were narrowed down, the next step was to review the flap schedule of blade #1 to ensure accordance with HQP requirements (table 1). Measured amplitudes and phases of the first six harmonics from blade #1 were analyzed and compared with HQP-specified requirements as shown in table 5. The flap deflection in RDMS, however, is expressed by $\delta_k(\psi_k) = \Sigma_n \beta_n \cdot \cos(n \cdot \psi_k - \phi_{n\ RDMS})$. To be consistent with HQP specifications (table 1), phase angles in table 5 were converted to Boeing's convention. Active-flap excitations for the other four blades are similar and consistent with blade #1 throughout the test (Appendix B). The selected points are shown to meet the flap conditions, with the exception of run 42, points 113 and 114, of the SMART1 case. These two points did not reach the 2°

amplitude specified by HQP. Due to this inconsistency, these two points were not considered for validation with predictions.

Once it was determined that all selected points met HQP requirements, the final step was the selection of a representative point for each case. The process began by first reviewing the mean statistical value for the collective, lateral, and longitudinal control inputs. Initial efforts focused on whether these control parameters were held constant during multiple repeated test points. Then the rotor performance data were examined. Since the pitchlink and the pitchcase were modeled in the predictions, only weight-tare correction was applied to the rotor balance data. The correction subtracted the effect of gravity acting on the rotor balance at non-zero shaft angle of attack. To select a single representative data point, the mean values for each of the rotor performance channels were tabulated for each of the four test cases. The value that was the closest to this calculated mean value was selected for each case. Due to inconsistencies in the pitch and roll moments, these channels were not used in the selection process, even though it was determined that the inconsistencies were small, given the measurement units, and the variations were insignificant. The data point that had the most selected values was chosen as the representative data point. For every case other than SMART1, there was clearly one point that would be selected for validations as marked in table 6. Because of the inconsistencies discovered when reviewing the flap requirements, the SMART1 case was narrowed down to two points, making the means of selection used thus far inadequate. Run 46, point 92, was selected as the representative point for the SMART1 case because the point met HQP requirements better than run 46, point 93. Table 7 displays the test points selected for each of the four flight cases.

TABLE 4. MEAN VALUES OF DATA POINTS BASED ON HQP REQUIREMENTS (IN GRAY SHADING)

		DARPA HQP points						
Run	Pt.	μ	α_{sc}	Ω	M_{tip}	M_{adv}	C_T/σ	C_P/σ
MDART		**0.300**	**-9.10**			**0.805**	**0.080**	
42	**106**	0.300	-9.12	392.2	0.620	0.805	0.079	0.0073
42	**111**	0.301	-9.11	392.3	0.620	0.805	0.081	0.0073
46	**86**	0.300	-9.11	392.3	0.620	0.805	0.082	0.0072
46	**90**	0.299	-9.11	392.4	0.620	0.805	0.080	0.0073
46	**94**	0.300	-9.11	392.4	0.620	0.805	0.080	0.0073
SMART1		**0.300**	**-9.10**			**0.805**	**0.080**	
42	**113**	0.300	-9.12	392.5	0.620	0.806	0.079	0.0074
42	**114**	0.301	-9.12	392.5	0.620	0.806	0.079	0.0074
46	**92**	0.300	-9.12	392.4	0.620	0.805	0.080	0.0074
46	**93**	0.300	-9.12	392.3	0.620	0.805	0.079	0.0074
SMART2		**0.300**	**-9.10**			**0.805**	**0.080**	
42	**108**	0.301	-9.11	392.1	0.619	0.805	0.082	0.0074
42	**109**	0.301	-9.11	392.1	0.619	0.805	0.081	0.0074
46	**89**	0.300	-9.11	392.3	0.620	0.805	0.082	0.0073
SMART3		**0.375**	**-9.10**			**0.852**	**0.070**	
		NA	NA	NA	NA	NA	NA	NA
SMART4		**0.200**	**1.50**			**0.746**	**0.075**	
42	**31**	0.202	1.50	392.7	0.621	0.746	0.075	0.0024
42	**32**	0.202	1.52	393.7	0.621	0.746	0.076	0.0024
61	**44**	0.198	1.52	401.2	0.624	0.747	0.073	0.0020
61	**45**	0.198	1.53	401.3	0.624	0.747	0.075	0.0020
61	**47**	0.198	1.54	401.3	0.624	0.747	0.076	0.0020
61	**48**	0.198	1.54	401.3	0.624	0.747	0.076	0.0020

TABLE 5. COMPARISON OF MEASURED AND HQP REQUIREMENTS OF THE FIRST SIX HARMONICS FOR THE ACTIVE FLAP OF BLADE #1

Harmonic amplitude (β_n) and phase (ϕ_n) of blade #1's active flap

Harm. *n*		0th		1st		2nd		3rd		4th		5th		6th	
Run	Pt	β_0	ϕ_0	β_1	ϕ_1	β_2	ϕ_2	β_3	ϕ_3	β_4	ϕ_4	β_5	ϕ_5	β_6	ϕ_6
MDART		**0.00**		**0.00**		**0.00**		**0.00**		**0.00**		**0.00**		**0.00**	
42	106	0.03	-	0.00	56.63	0.00	206.74	0.00	115.05	0.00	331.06	0.00	119.05	0.00	116.86
42	111	0.02	-	0.01	75.33	0.00	114.84	0.00	102.15	0.00	150.54	0.00	99.16	0.00	44.27
46	86	0.03	-	0.00	344.19	0.00	209.08	0.00	109.38	0.00	355.60	0.00	252.42	0.00	185.16
46	90	0.03	-	0.00	192.98	0.01	75.06	0.00	171.35	0.00	202.58	0.00	37.32	0.00	190.59
46	94	0.03	-	0.00	148.68	0.01	103.47	0.01	296.43	0.00	110.97	0.01	239.64	0.01	231.46
SMART1		**0.00**		**0.00**		**0.00**		**0.00**		**0.00**		**2.00**	**90.00**	**0.00**	
42	113	0.03	-	0.00	262.91	0.00	296.68	0.00	155.17	0.00	96.58	1.72	89.27	0.00	268.77
42	114	0.02	-	0.00	159.29	0.01	4.13	0.01	268.83	0.01	173.45	1.71	89.26	0.01	241.63
46	92	0.02	-	0.00	156.12	0.00	183.00	0.00	71.55	0.00	124.46	1.99	93.88	0.00	341.17
46	93	0.03	-	0.00	213.17	0.00	278.83	0.00	166.40	0.01	83.33	1.99	94.09	0.00	265.08
SMART2		**0.00**		**0.00**		**0.00**		**2.00**	**60.00**	**0.00**		**0.00**		**0.00**	
42	108	0.03	-	0.00	180.27	0.00	92.12	1.98	62.35	0.00	195.41	0.00	357.90	0.00	231.54
42	109	0.03	-	0.00	192.75	0.01	349.83	1.97	62.41	0.01	204.73	0.00	319.32	0.00	238.88
46	89	0.03	-	0.00	128.80	0.00	338.59	1.97	62.40	0.01	200.29	0.00	128.85	0.00	197.41
SMART3		**0.00**		**0.00**		**0.00**		**0.00**		**0.00**		**1.00**	**180.00**	**0.00**	
		NA	NA	NA	NA	NA	NA	NA	NA	NA	NA	NA	NA	NA	NA
SMART4		**0.00**		**0.00**		**2.00**	**240.00**	**0.00**		**0.00**		**1.00**	**330.00**	**0.00**	
42	31	0.01	-	0.00	314.80	1.97	241.57	0.01	21.93	0.01	309.79	1.00	334.01	0.00	111.16
42	32	0.01	-	0.00	193.15	1.97	241.30	0.01	357.97	0.00	222.77	0.99	333.27	0.00	88.52
61	44	0.01	-	0.00	227.79	2.00	241.71	0.01	9.84	0.00	142.29	0.99	334.20	0.07	129.81
61	45	0.01	-	0.00	251.55	2.00	241.80	0.01	14.59	0.00	168.45	1.00	334.35	0.07	134.42
61	47	0.01	-	0.00	237.03	1.99	241.49	0.01	3.46	0.01	80.34	1.00	333.98	0.01	91.07
61	48	0.01	-	0.01	290.85	1.99	241.76	0.00	66.49	0.00	253.82	1.00	334.59	0.00	36.03

TABLE 6. ROTOR PERFORMANCE DATA FOR TEST AND RUN-POINT EVALUATION

Representative data point selection process using rotor performance data

Run	Pt	COLLA	LATA	LONGA	ROTOR DRAGRH	ROTOR SIDERH	ROTOR LIFTRH	ROTOR TORQUE	ROTOR ROLLRH	ROTOR PITCHRH
MDART										
42	106	10.6	-1.8	6.3	-32.4	-133.4	5950	110968	3757	9379
42	111	10.7	-1.6	6.2	-39.1	-120.0	6060	111755	6254	9803
46	86	10.6	-1.6	5.9	-17.5	-138.4	6117	109606	6837	15506
46	90	10.6	-1.6	6.1	-66.3	-139.0	5985	109988	6264	11351
46	**94**	10.6	-1.6	6.1	-63.3	-138.5	6003	110094	6356	11551
	MEAN	NA	NA	NA	-43.7	-133.9	6023	110482	NA	NA
SMART1										
46	**92**	10.6	-1.6	6.1	-75.8	-141.0	5944	112332	5879	9446
46	93	10.6	-1.6	6.1	-74.0	-137.9	5929	112413	6181	9877
	MEAN	NA	NA	NA	-74.9	-139.5	5937	112373	NA	NA
SMART2										
42	**108**	10.7	-1.8	6.4	-17.0	-145.2	6129	113126	803	10697
42	109	10.7	-1.6	6.5	-47.8	-129.1	6080	113214	2504	8064
46	89	10.6	-1.6	6.1	-20.5	-148.5	6144	110896	3072	14657
	MEAN	NA	NA	NA	-28.4	-140.9	6118	112412	NA	NA
SMART3										
		NA	NA	NA	NA	NA	NA	NA	NA	NA
SMART4										
42	31	4.7	-2.0	2.6	-178.3	-165.1	5730	37415	988	7992
42	**32**	4.8	-2.0	2.6	-171.7	-167.3	5839	37431	1408	6955
61	44	4.7	-1.9	2.6	-183.1	-165.4	5637	37987	1126	7913
61	45	4.7	-1.9	2.6	-183.5	-167.1	5766	37230	1370	7436
61	47	4.7	-2.1	2.5	-161.3	-177.1	5843	37265	165	9236
61	48	4.7	-2.1	2.5	-163.3	-177.6	5853	37248	70	8941
	MEAN	NA	NA	NA	-173.5	-169.9	5778	37429	NA	NA

Gray shading = point that is closest to mean; **Bold** = representative data point.

TABLE 7. SUMMARY OF FINAL SELECTED POINT FOR EACH TEST CASE

	Run	Point
MDART	46	94
SMART1	46	92
SMART2	42	108
SMART3	NA	NA
SMART4	42	32

In addition to using mean statistical data associated with the rotor and flap settings, 64-revolution-averaged time histories were also examined to check for temporal consistencies over a rotor revolution. For the final selected points, it was necessary to confirm that they were repeatable for each revolution of data. For each flight case, the flap schedules, in-plane acoustics, rotor performance, and structural loads were plotted in groups (see Appendices B to F). The data presented in this report includes both static and oscillatory components. For blade structural loads, the static components are not reliable because of bias from centrifugal loading. A listing of all HQP and RDMS channel names, units, and descriptions used for data acquisition, along with the coordinate conventions used during data analysis, can be found in Appendix A. In reviewing these repeatability plots, the mean time histories generally demonstrated highly repeatable temporal characteristics, except for the following cases/channels:

- SMART1 case for run 42, points 113 and 114, did not achieve the specified flap amplitude during testing, but came within 87% of the target amplitude. These test points were discarded from subsequent considerations.
- M14 shows highly inconsistent variations in the acoustic data. This is most likely associated with strong wall reflections due to its location situated outside of the acoustic-liner section of the tunnel. Microphone M14 is not recommended for use in the analysis.
- SMART4 flight case showed more variability than other flight cases in all areas due to strong blade-vortex interaction occurrences. As will be shown in the following section, this variability stayed within the standard deviations.

Overall, these plots confirmed that the HQP cases were indeed repeatable, and the individual selected test points are representative of the state of the rotor apt for HQP Phase Ib code validation.

Data Quality and Reporting Format

Once the representative test point had been selected for each of the HQP test cases, the "unsteadiness" of each channel measurement associated with dynamic variations in rotor/wind tunnel operations are evaluated. The objective is to obtain an appropriate scatter-band that will be useful for correlating experimental data to HQP predictions. For this purpose, the standard derivations derived from variations between revolution-to-revolution, over the entire 64-revolution duration of measurement, were computed for each channel (see Appendices C to F). This exercise yielded the following results:

- With the exception of microphone and some rotor balance/blade channels, all measurements yielded highly consistent and stable measurements during the 64-revolution duration with acceptable small scatter-band.
- Microphone channels in general were found to have larger scatter-bands than other channels. This is especially apparent for microphone M15 where the measured rotor noise signal is obscured by large amplitude fluctuations manifesting at very low frequencies (fig. 5(a)). Further examination revealed that these low-frequency contents are associated with the background noise of the facility and instrumentation self-noise, and are not directly due to the operation of the rotor. To remove these non-rotor-related noise content, a band-pass filter, which filtered out the non-integer harmonics up to 3/rev, was applied to the entire 64 revolutions of data, prior to revolution-based averaging. As shown in figure 5(b), this band-pass approach significantly reduces the scatter-band, but does not affect the 64-revolution averaged time history. (Note: All acoustic channel plots shown in Appendices C to F reflect the effects of the band-pass filter.)
- Fluctuations in some of the rotor performance channels were observed. Analyses revealed a strong contribution from a subharmonic frequency that was not rotor related, but was attributed to a rotating gear frequency at 2405/392 = 6.135 per rev (ref. 6). The net result introduced large in-plane vibratory load fluctuations that amplified error bands in the rotor balance measurements for drag force, side force, pitching moment, and rolling moment channels as shown in figure 6(a). This subharmonic, however, has no effect on the averaged revolution and the integer harmonics. Nevertheless to correct for the problem, a band-pass filter was developed to remove the 6.135-per-rev subharmonic in the rotor performance channels as shown in figure 6(b). Subsequent results yielded smaller standard deviations that implied a highly steady-state condition throughout the 64 revolutions of data acquisition. (Note: All drag force, side force, pitching moment, and rolling moment channel plots shown in Appendices C to F reflect the effects of this band-pass filter.)
- Measurements on the flex-beam torsion sensor of blade #1 were dominated by a strong one-per-rev variation with very small standard deviations. Subsequent analyses determined that this is caused by the pitchcase, which accentuated effects of the swash-plate motion associated with cyclic motion. Very little effects due to aeroelastic blade motion were registered at this flex-beam sensor. Because the variations in the control inputs between individual revolutions were small (see Appendices C to F), this resulted in very small standard deviation for this flex-beam torsion sensor.

(a)

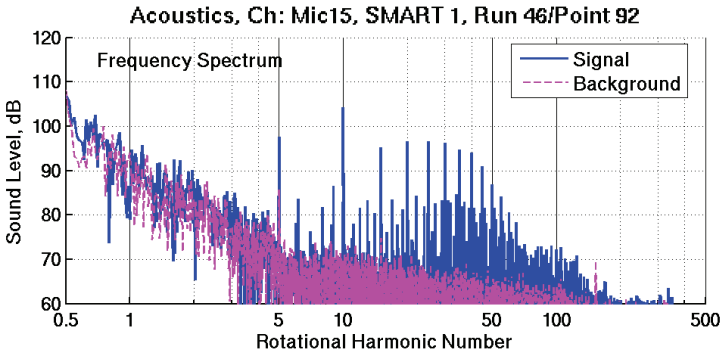

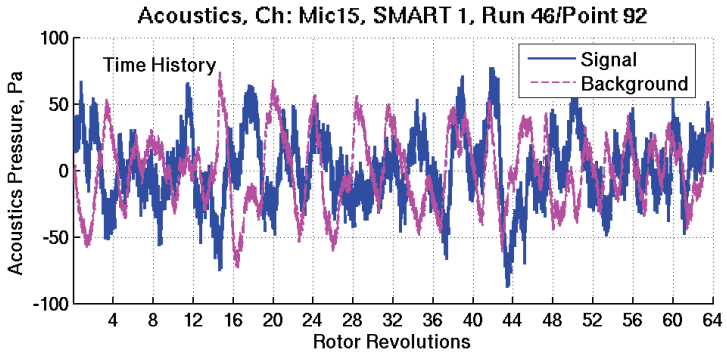

(b)

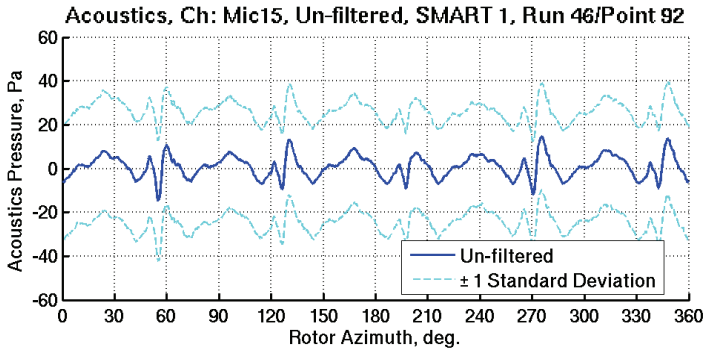

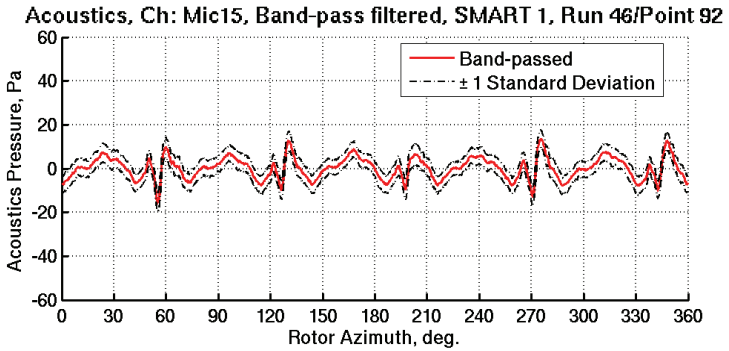

Figure 5. Acoustic data from Microphone 15 for SMART 1 case: a) Signal-to-background noise comparisons, b) Effect of applying band-pass filter to remove non-rotor-related noise sources.

(a)

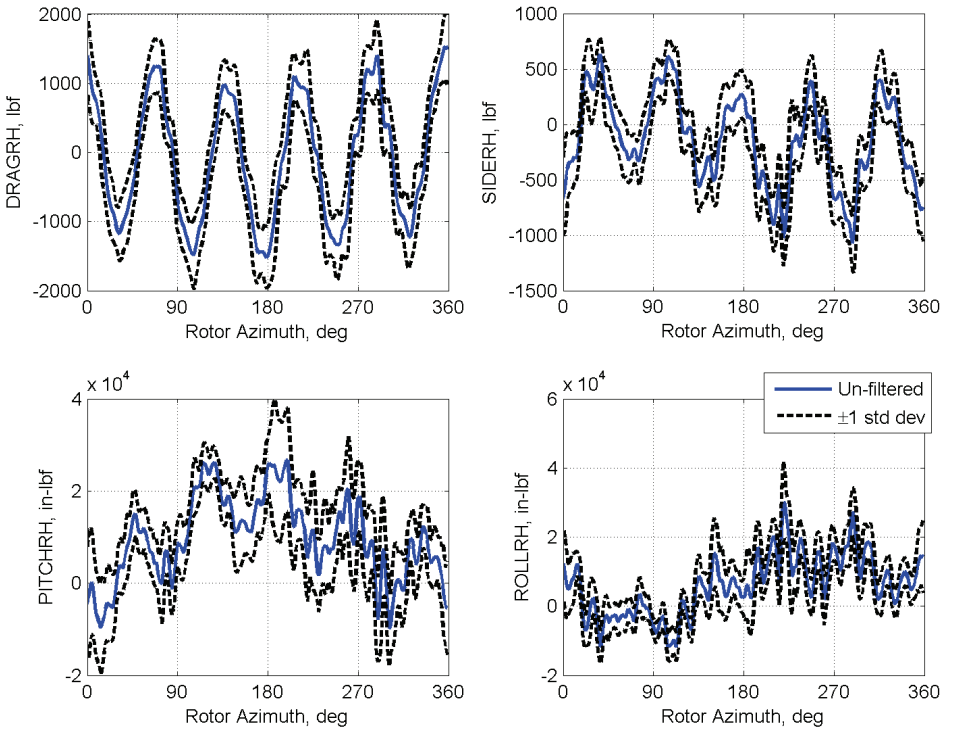

(b)

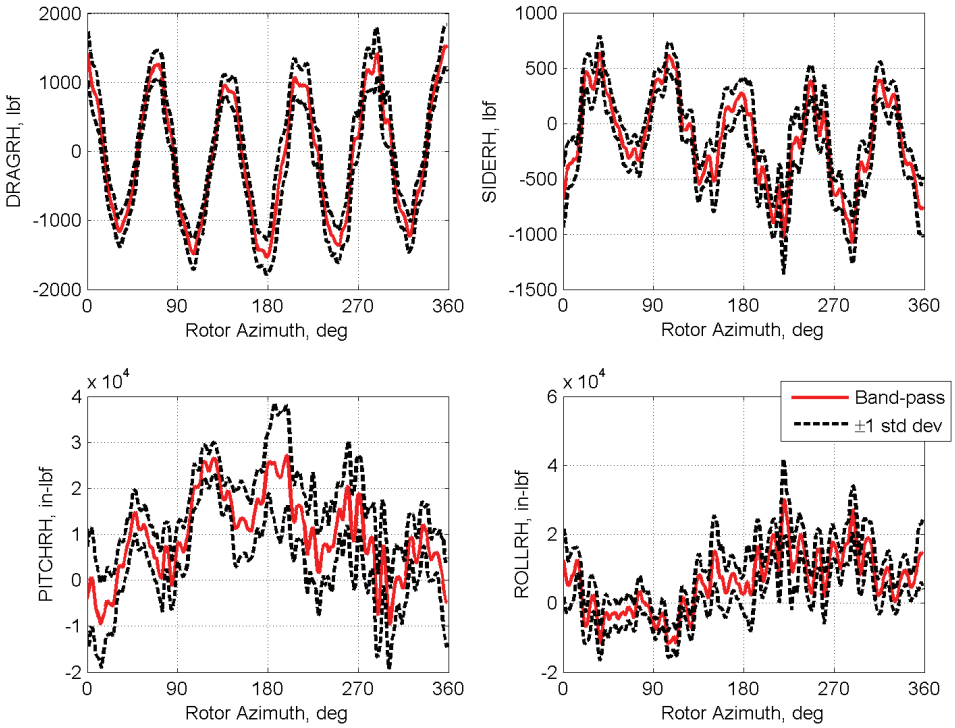

Figure 6. Rotor performance data: a) Unfiltered, b) Filtered.

Conclusion

- Data collected from the Boeing-SMART rotor test were examined and formatted to meet requirements as stated by DARPA for the HQP Phase Ib code validation effort. All the pertinent experimental data channels were reviewed to ensure HQP requirements were met and that the quality and repeatability of the data was adequate.

- One representative test point for each of the five flight conditions was selected from multiple repeats for submission to DARPA. Overall, it was determined that each individual selected test point was representative of the desired state of the rotor and was apt for HQP Phase Ib code validation.

- In analyzing these data, contributions from non-rotor-related sources (e.g., instrumentation noise–and facility effects) were found to impact data quality. These discrepancies were rectified via implementation of band-pass filters during data post-processing to remove unnecessary information not related to rotor.

- Information, both mean statistics and mean time histories, for each data point chosen has been formatted to meet HQP requirements and is enclosed in a CD attached to this report. Information on the error band of each measurement channel was examined and presented as well.

References

1. Newman, D.; Doligalski, T.; and Minniti, R.: Advances in Modeling and Simulation of Rotorcraft Noise and Associated Impacts on Survivability. 26th Army Science Conference, Orlando, Fla., Dec. 2008.
2. Jacklin, S.A.; Lau, B. H.; Nguyen, K. Q.; Smith, R. L.; and McNulty, M. J.: Full-Scale Wind Tunnel Test of the McDonnell Douglas Five-Bladed Advanced Bearingless Rotor: Performance, Stability, Loads, Control Power, Vibration, and HHC Data. AHS Aeromechanics Specialist Conference, San Francisco, Calif., Jan. 1994.
3. Helicopter Quieting Report Phase Ib Reporting Guideline (see attached CD).
4. Sim, B. W.; JanakiRam, R. D.; Barbely, N. L.; and Solis, E.: Reduced In-Plane, Low Frequency Noise of an Active Flap Rotor. ASH 65th Annual Forum, Grapevine, Tex., May 2009.
5. Straub, F. and Anand, V. R.: SMART Rotor Extended Wind Tunnel Test Plan Draft and Closed Loop Control Methodologies Report. Report L9S7-05-DTP-08001, CDRL 5-2, Flight Technology Technical Note FTN-2008-010, The Boeing Company, Feb. 2008.
6. Hall, S. R.; Anand, V. R.; Straub, F. K.; and Lau, B. H.: Active Flap Control of the SMART Rotor for Vibration Reduction. AHS 65th Annual Forum, Grapevine, Tex., May 2009.
7. Straub, F. K.; Anand, V. R.; Birchette, T. S.; and Lau, B. H.: Wind Tunnel Test of the SMART Active Flap Rotor. AHS 65th Annual Forum, Grapevine, Tex., May 2009.
8. Anand, V. R. and Straub, F.: SMART Rotor Wind Tunnel Test-Software Plan. Report L9S7-03-FTP-08002, CDRL 3-2, Flight Technology Technical Note FTTN-2008-003, The Boeing Company, Jan. 2008.
9. Straub, F., et al.: Development and Whirl Tower Test of the SMART Active Flap Rotor. SPIE Conf. on Smart Material and Structures, San Diego, Calif., 2004.
10. Schmitz, F. H.: Rotor Noise. Ch. 2 in book by Hubbard, H. H., Aeroacoustics of Flight Vehicles, Theory and Practice, Vol. 1: Noise Sources, Published for the Acoustical Society of America through the American Institute of Physics, 1995.

Appendices

Appendix A

Channel Description

Appendix A subdivides test data and relates HQP and RDMS channel names. This table includes channel units, the positive directions defined in RDMS, and channel descriptions. The rotor performance channels with weight-tare correction are referenced to the hub center. LIFTRH and THRUST are identical and used interchangeably throughout this report. In RMDS channel names, a "_B" indicates Boeing measurement, instead of NFAC measurement.

Folder/File Label	RMDS	HQP	RDMS units (positive direction)	Description
Acoustics	MIC_13	M0159	Pascal (compression)	
	MIC_14	M0156	Pascal (compression)	
	MIC_15	M0180	Pascal (compression)	
Control Inputs	COLLA	COLLECTIVE	deg (nose up)	Rotor collective control input
	LONGA	LONGITUDINAL	deg (nose down at ψ=90°)	Rotor longitudinal control input
	LATA	LATERAL	deg (nose down at ψ=0°)	Rotor lateral control input
	ALFSC	ALPHA	deg (rotor shaft tilt aft)	Corrected model shaft angle of attack
Rotor Performance	DRAGRH	X_Force	lbf (aft)	Rotor drag force
	SIDERH	Y_Force	lbf (right)	Rotor side force
	LIFTRH, THRUST	Z_Force	lbf (up)	Rotor lift force
	ROLLRH	X_Moment	in-lbf (right down)	Rotor roll moment
	PITCHRH	Y_Moment	in -lbf (nose up)	Rotor pitch moment
	TORQ	Z_Moment	in -lbf (drag)	Rotor torque
Structural Loads/Pitch	MRPLK1LOAD	STA010	lbf (tension)	Main Rotor Pitchcase 1 Pitchlink Load
Structural Loads/Chord	MRFBM1CB26P5	STA026	in -lbf (lag)	Main Rotor Flexbeam 1 Chord Bending Station 26.5
	MRPC1CB33P25	STA033	in -lbf (lag)	Main Rotor Pitchcase 1 Chord Bending Station 33.25
	MRBLD1CB42P75	STA042	in -lbf (lag)	Main Rotor Blade 1 Chord Bending Station 42.75
	MRBLD1CB70	STA070	in -lbf (lag)	Main Rotor Blade 1 Chord Bending Station 70
	MRBLD1CB120	STA120	in -lbf (lag)	Main Rotor Blade 1 Chord Bending Station 120
	MRBLD1CB164	STA164	in -lbf (lag)	Main Rotor Blade 1 Chord Bending Station 164
Structural Loads/Flap	MRFBM1FB9	STA009	in -lbf (tip up)	Main Rotor Flexbeam 1 Flap Bending Station 9
	MRPC1FB33P25	STA033	in -lbf (tip up)	Main Rotor Pitchcase 1 Flap Bending Station 33.25
	MRBLD1FB42P75	STA042	in -lbf (tip up)	Main Rotor Blade 1 Flap Bending Station 42.75
	MRBLD1FB70	STA070	in -lbf (tip up)	Main Rotor Blade 1 Flap Bending Station 70
	MRBLD1FB87	STA087	in -lbf (tip up)	Main Rotor Blade 1 Flap Bending Station 87
	MRBLD1FB120	STA120	in -lbf (tip up)	Main Rotor Blade 1 Flap Bending Station 120
	MRBLD1FB164	STA164	in -lbf (tip up)	Main Rotor Blade 1 Flap Bending Station 164
	MRBLD1FB180	STA180	in -lbf (tip up)	Main Rotor Blade 1 Flap Bending Station 180
Structural Loads/Torsion	MRPC1TOR25P5	STA025	in -lbf (leading edge up)	Main Rotor Pitchcase 1 Torsion Station 25.5
	MRFBM1TOR26P5	STA026	in -lbf (leading edge up)	Main Rotor Flexbeam 1 Torsion Station 26.5
	MRBLD1TOR51	STA051	in -lbf (leading edge up)	Main Rotor Blade 1 Torsion Station 51
	MRBLD1TOR71	STA071	in -lbf (leading edge up)	Main Rotor Blade 1 Torsion Station 71
	MRBLD1TOR130	STA130	in -lbf (leading edge up)	Main Rotor Blade 1 Torsion Station 130
	MRBLD1TOR164	STA164	in -lbf (leading edge up)	Main Rotor Blade 1 Torsion Station 164
Flight Conditions	MU_B	MU	-	Advance ratio
	PS_B	P_INF	psi	Tunnel static pressure
	TSR_B	T_INF	deg Rankine	Tunnel static temperature
	RHO_B	RHO_INF	slug/ft^3	Tunnel air density
	CSND_B	SOUND_SPEED	ft/s	Speed of sound
	VFPS_B	V_FLIGHT	ft/s	Tunnel speed
	MTUN_B	MACH_INF	-	Tunnel Mach number
	MTIP_B	TIP_MACH	-	Hover tip Mach number
	CTOS	CT_SIGMA	-	Rotor thrust coefficient over solidity
	CPOS	CP_SIGMA	-	Rotor power coefficient over solidity

Appendix B

Flap-Schedule Polar Plot

Appendix B compares the measured harmonic amplitudes and phases of all five active flaps with the HQP requirement for each prescribed flap schedule (table 1) in the selected representative test points (table 7). The harmonic phases are presented in Boeing convention.

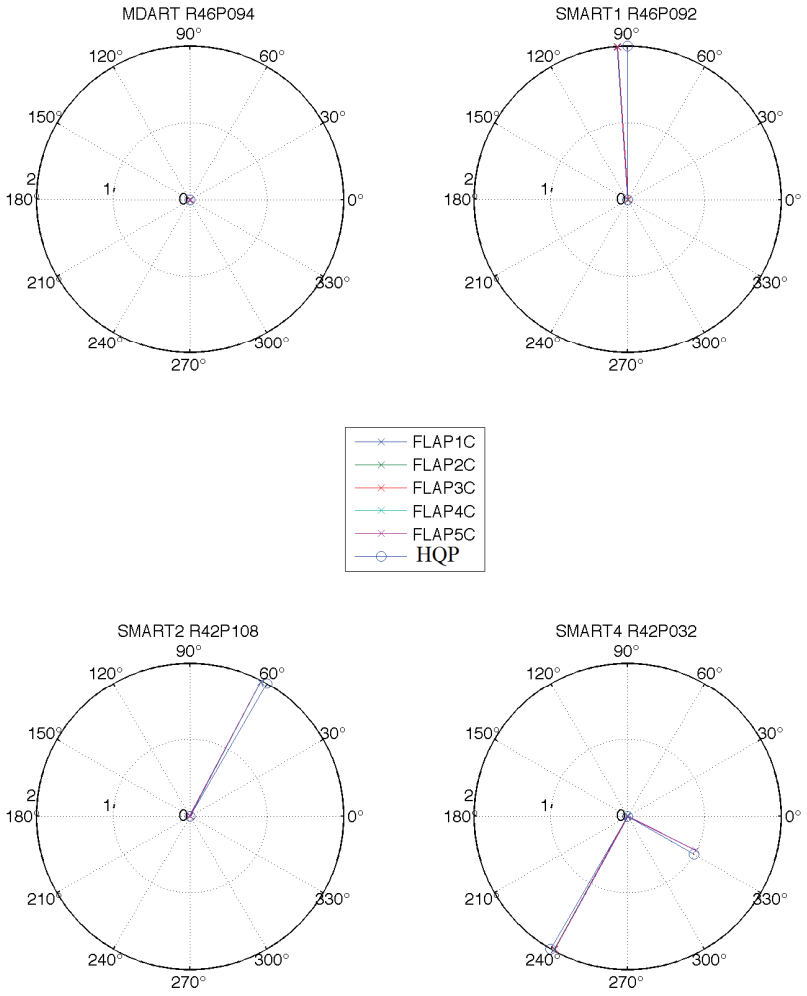

Figure B1. Polar plot of active-flap schedule.

Appendix C
MDART Summary Plots

In Appendix C, repeatability for all five MDART test points (table 4) was plotted along with the HQP requirements to show data regularity. These plots (figs. C1 to C7) include flap schedules of all five flaps, acoustics for the three in-plane microphones, rotor performance at the rotor hub, and structural loading on blade #1. Unless indicated, the azimuth for all plots is referenced to the azimuthal angle of blade #1. The thick line in figures C1 to C7 corresponds to the representative data point selected.

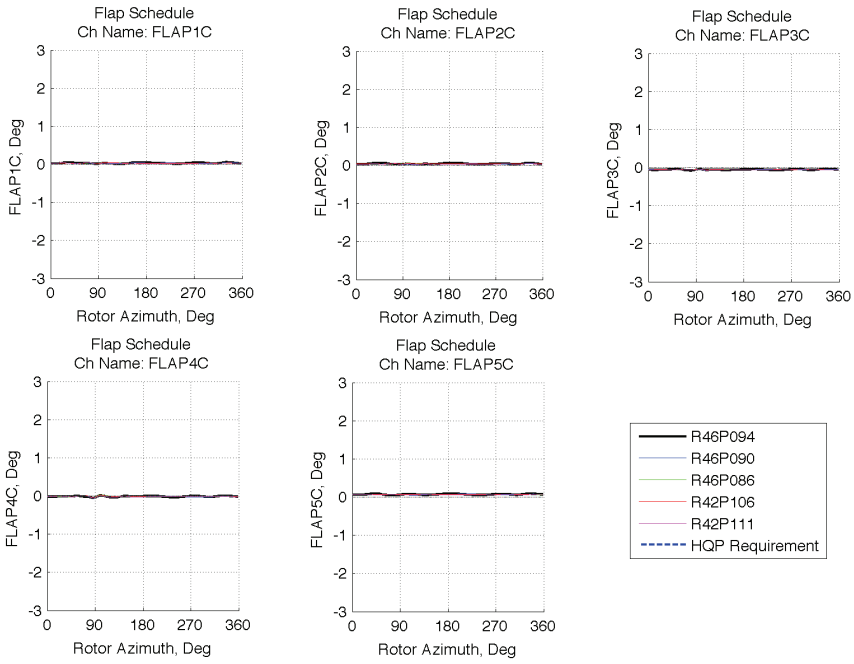

Figure C1.Comparison of measured active-flap schedule of blades #1 to #5 with HQP requirements, plotted against the local blade azimuth.

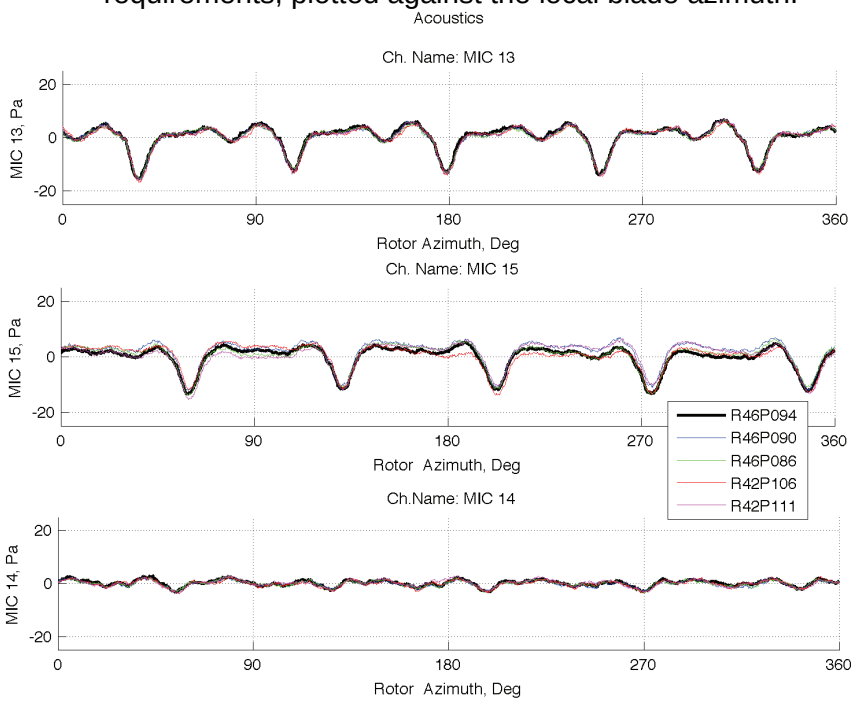

Figure C2. Microphones M13, M15, and M14.

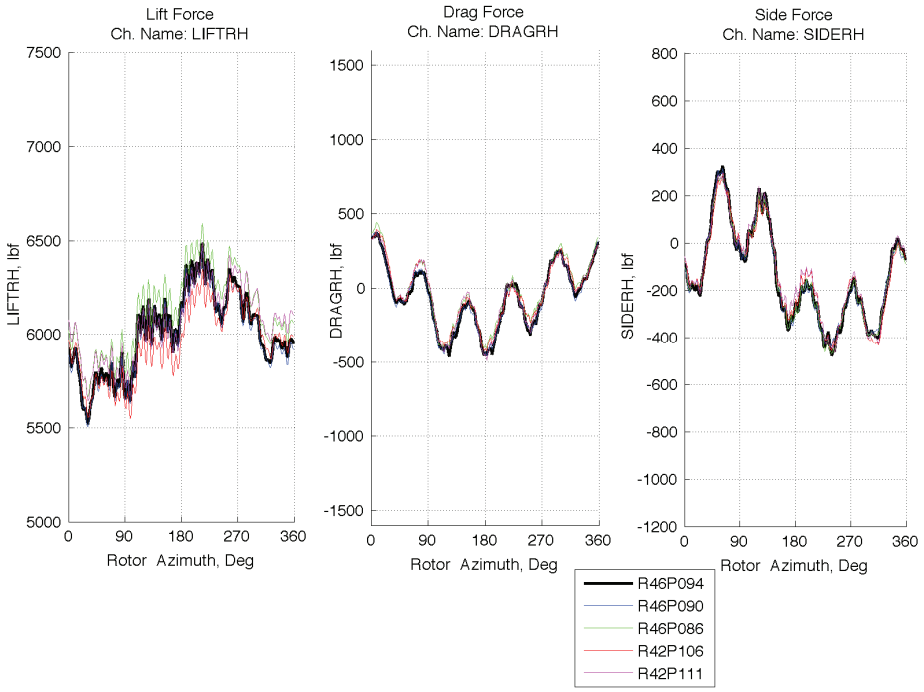

Figure C3. Lift, drag, and side forces at rotor hub.

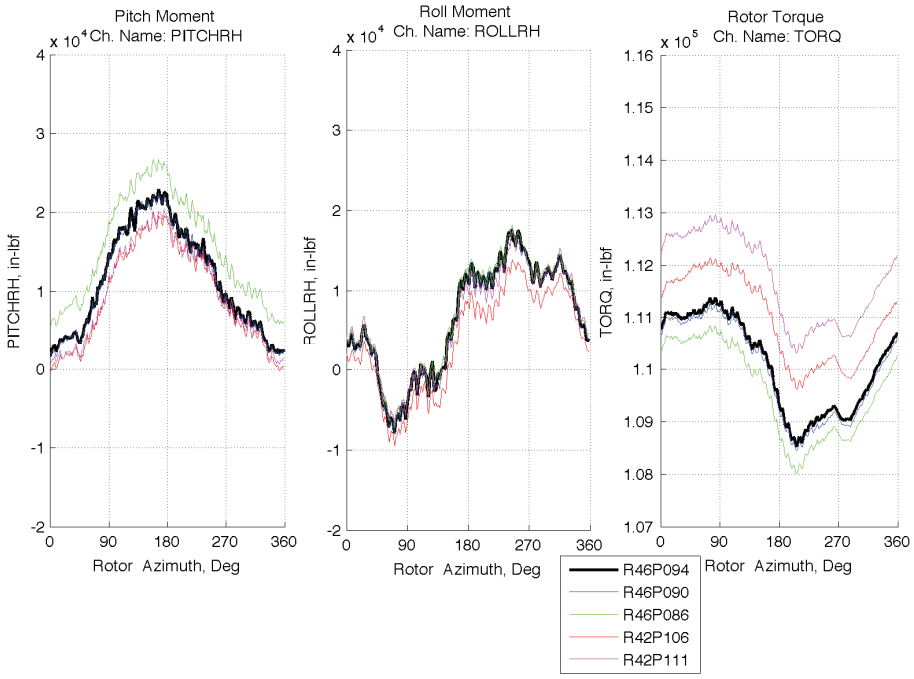

Figure C4. Pitching moment, rolling moment, and rotor torque at rotor hub.

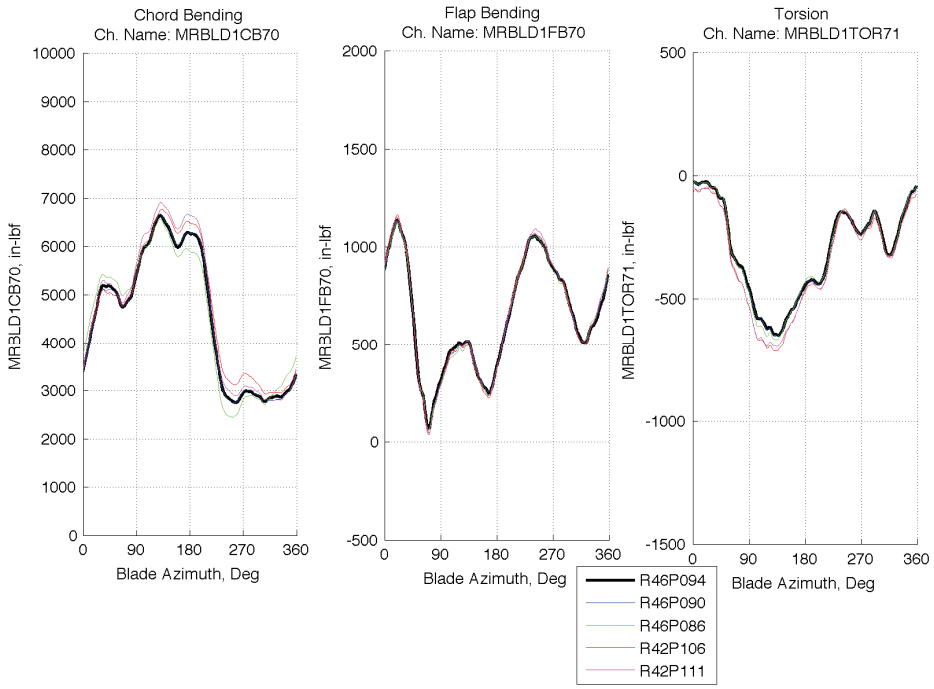

Figure C5. Blade chord- and flap-bending at station 70, and torsion at station 71.

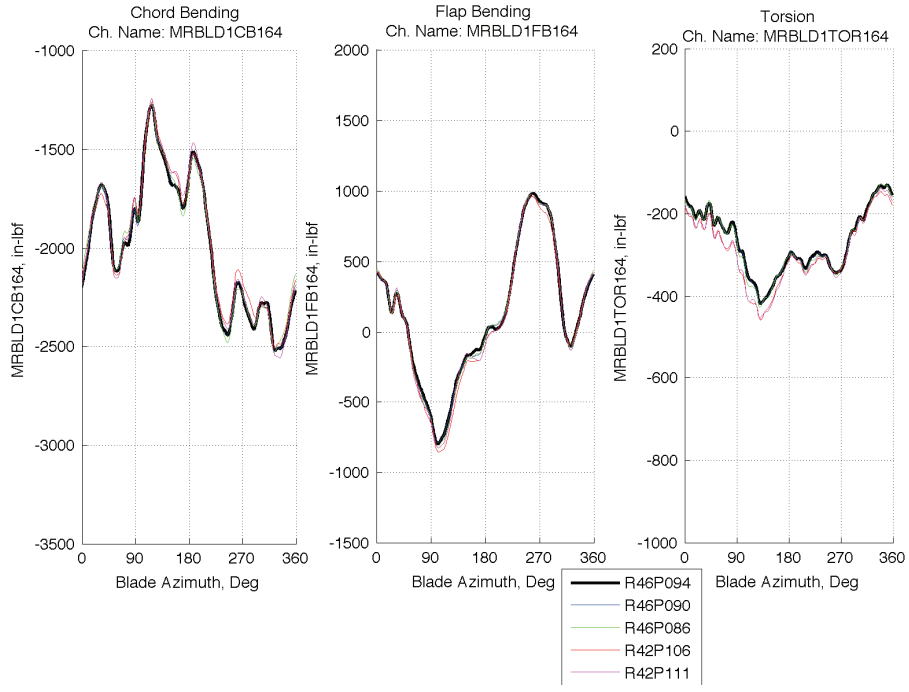

Figure C6. Blade chord-bending, flap-bending, and torsion at station 164.

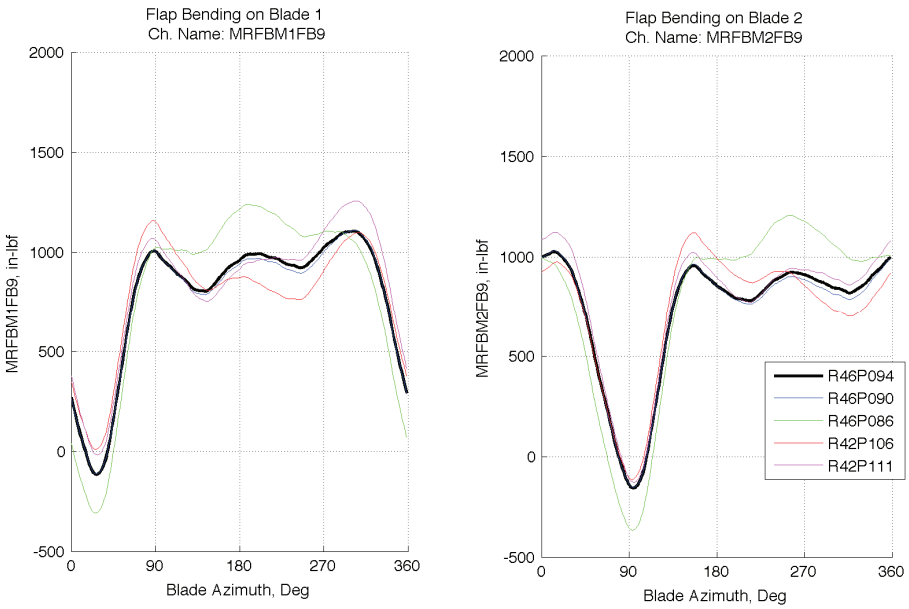

Figure C7. Flap bending of flexbeam 1 and 2 at station 9.

The standard deviations, calculated from 64 revolutions of data at each azimuth, are also plotted for all channels to show the appropriate scatter-band for the MDART case, and compared with the averaged revolution and a revolution synthesized from the integer harmonics (figs. C8 to C14). The three in-plane acoustic channels and the rotor channels (drag, side, roll, and pitch) are band-pass filtered prior to plotting.

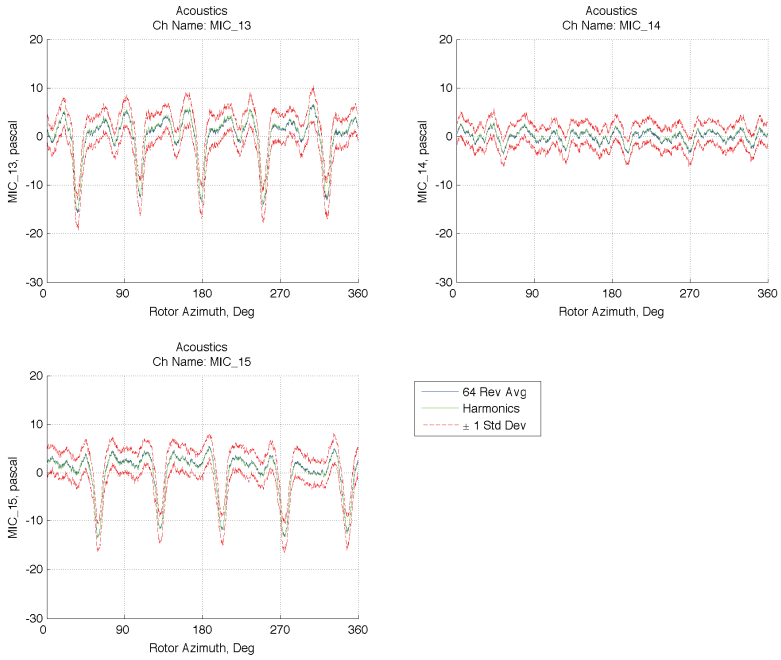

Figure C8. Standard deviation plots for acoustics.

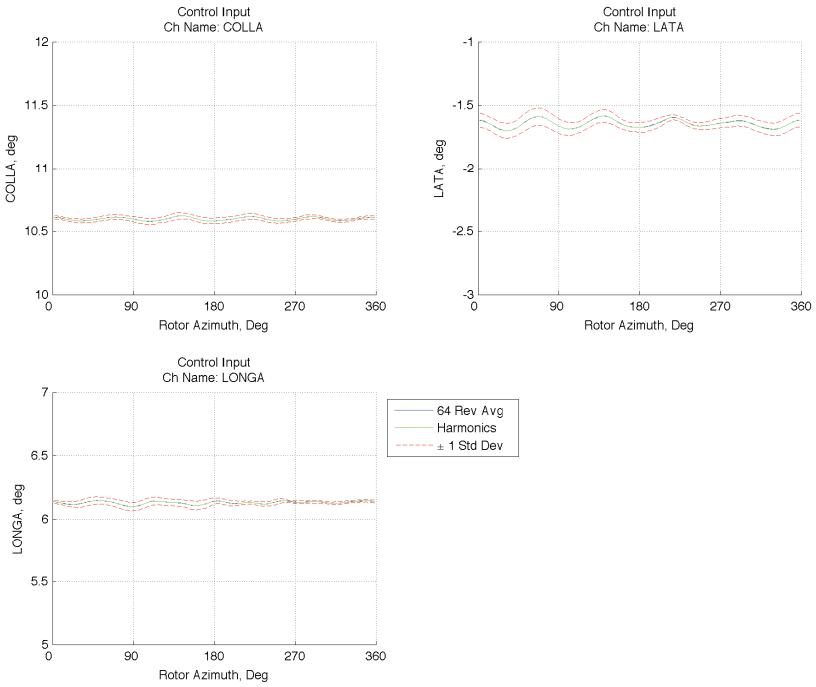

Figure C9. Standard deviation plots for control inputs.

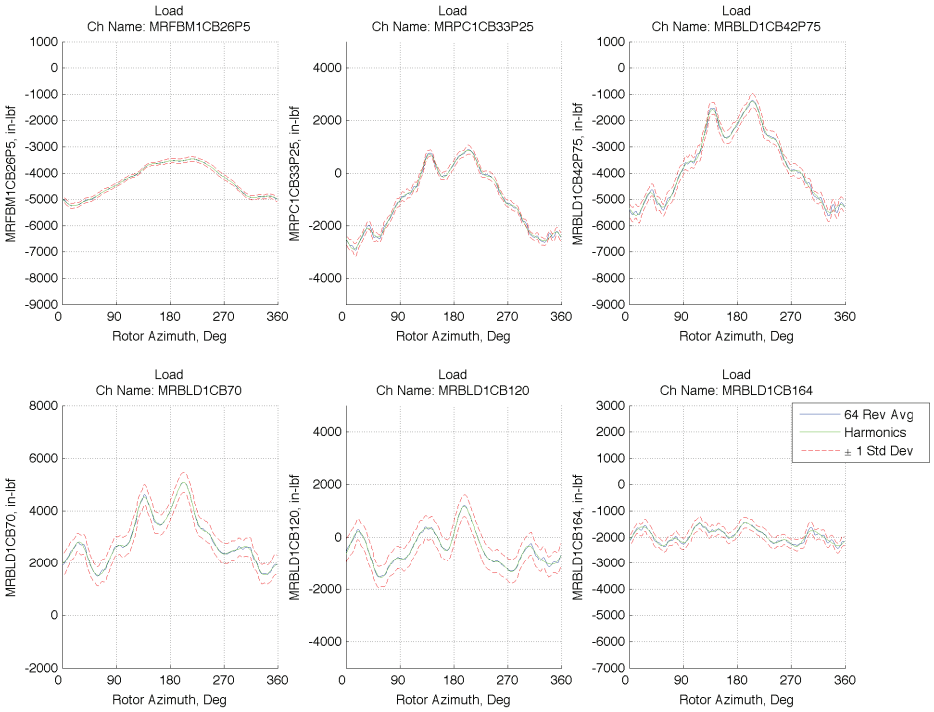

Figure C10. Standard deviation plots for chord-bending loads at various stations.

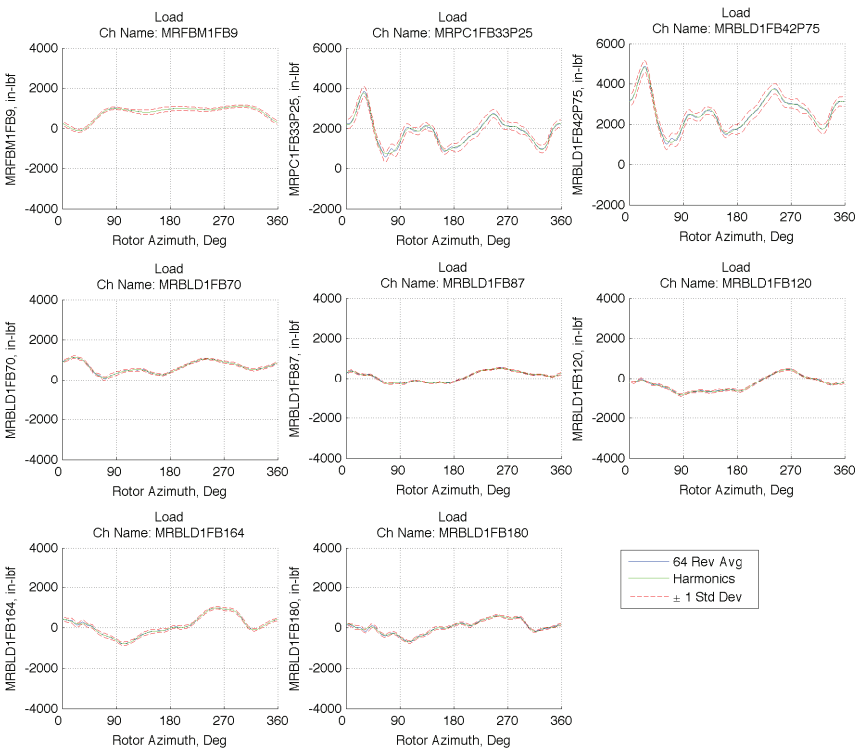

Figure C11. Standard deviation plots for flap-bending loads at various stations.

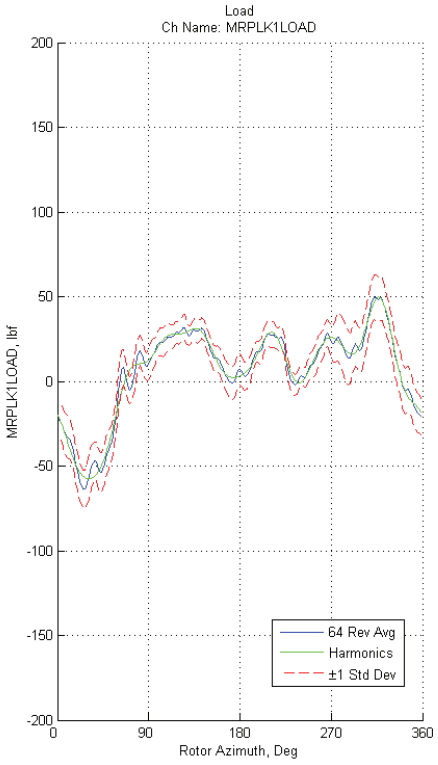

Figure C12. Standard deviation plot for pitch-link load.

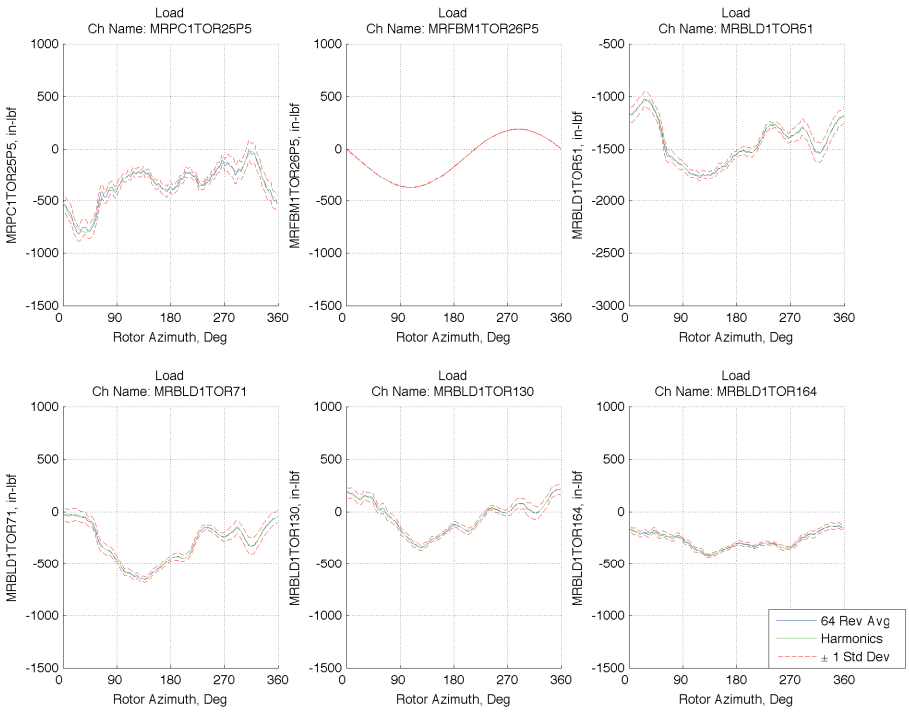

Figure C13. Standard deviation plots for torsion loads at various stations.

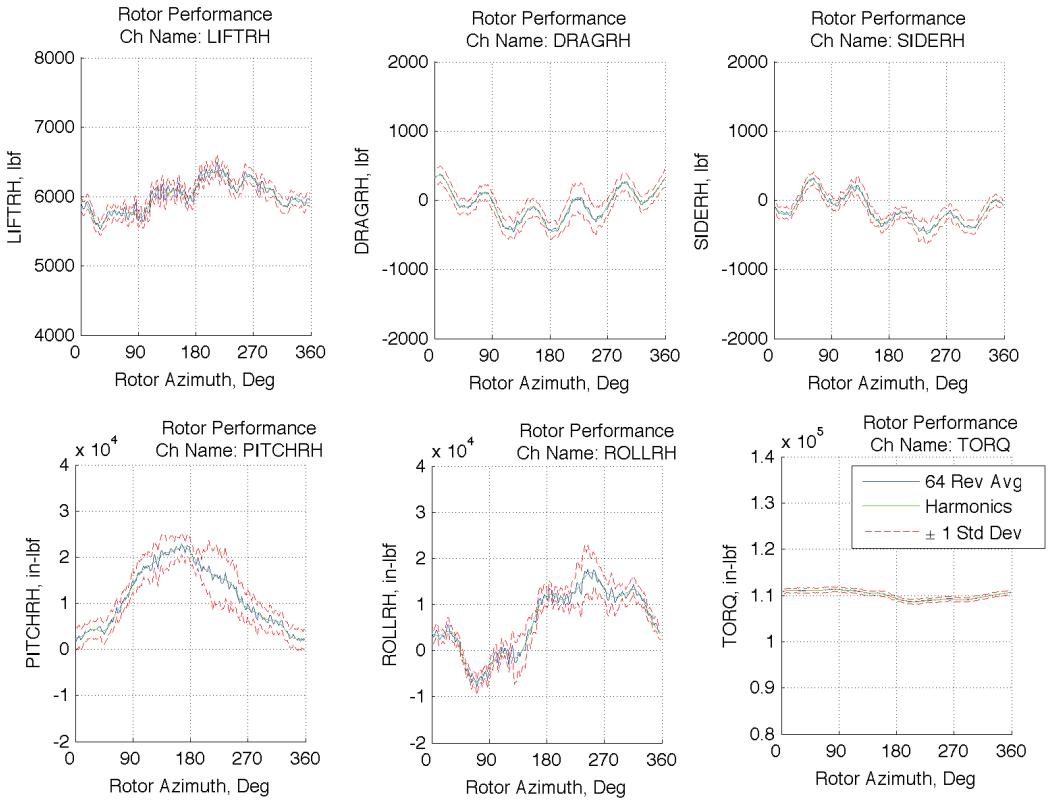

Figure C14. Standard deviation plots for rotor performance.

Appendix D

SMART1 Summary Plots

In Appendix D, repeatability for all four SMART1 test points (table 4) were plotted along with the HQP requirements to show data regularity. These plots (figs. D1 to D7) include flap schedules of all five flaps, acoustics for the three in-plane microphones, rotor performance at the rotor hub, and structural loading on blade #1. Unless indicated, the azimuth for all plots is referenced to the azimuthal angle of blade #1. The thick line in figures D1 to D7 corresponds to the representative data point selected.

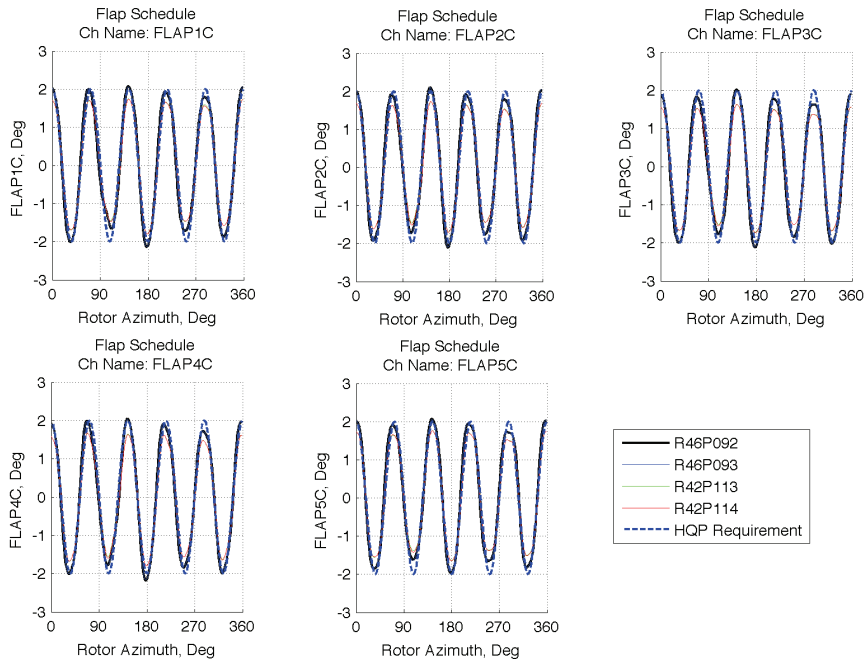

Figure D1. Comparison of measured active-flap schedule of blades #1 to #5 with HQP requirements, plotted against the local blade azimuth.

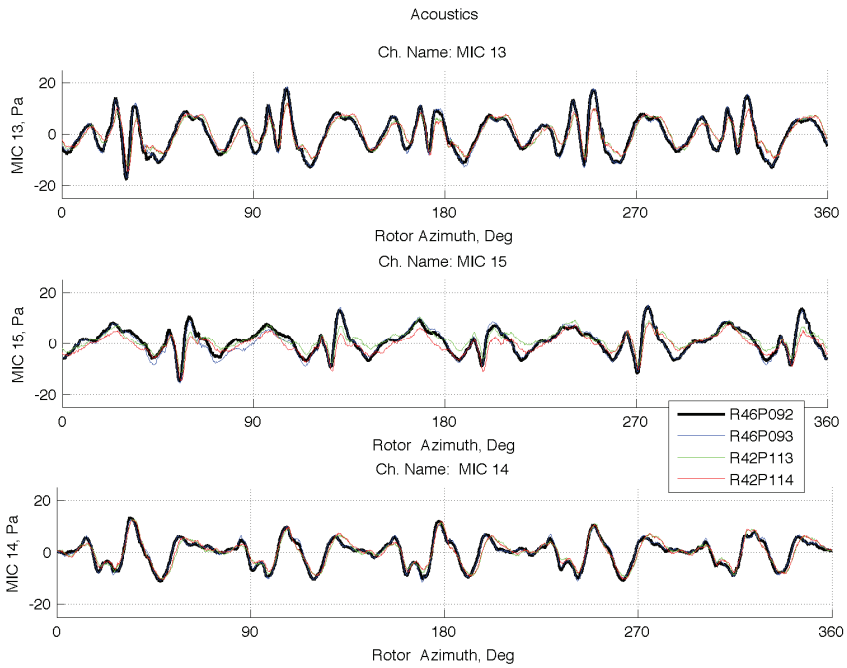

Figure D2. Microphone M13, M15, and M14.

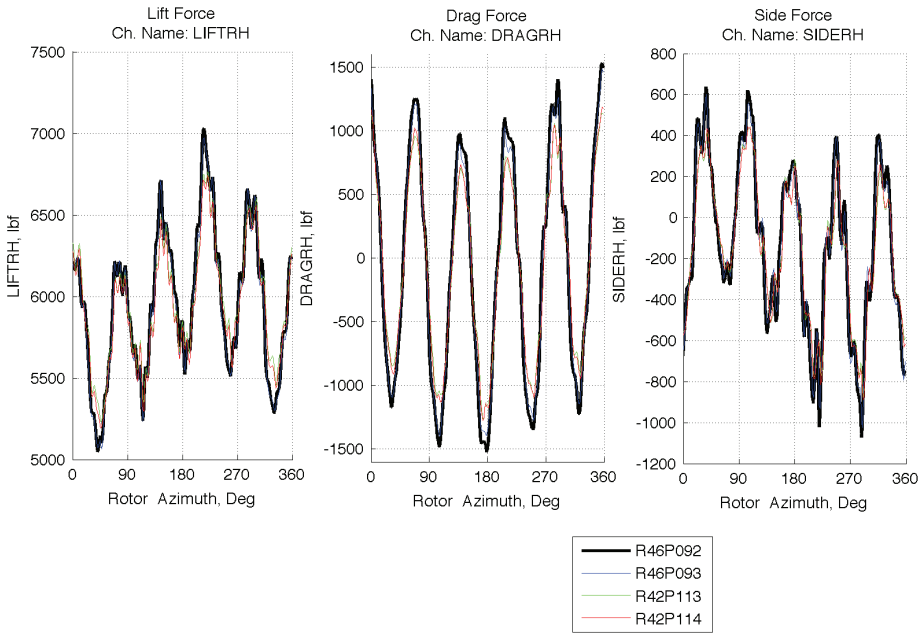

Figure D3. Lift, drag, and side forces at rotor hub.

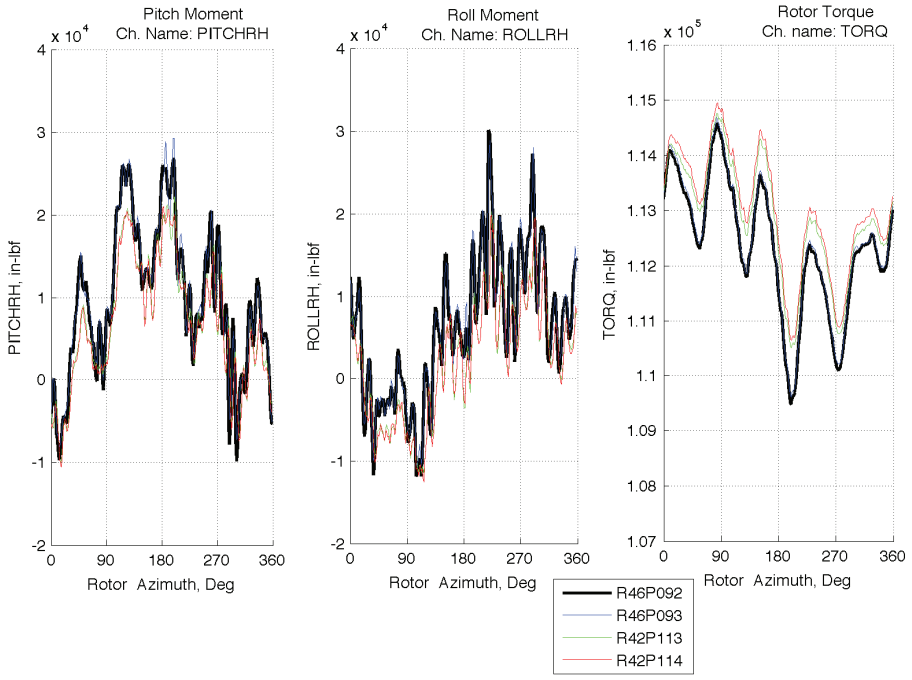

Figure D4. Pitching moment, rolling moment, and rotor torque at rotor hub.

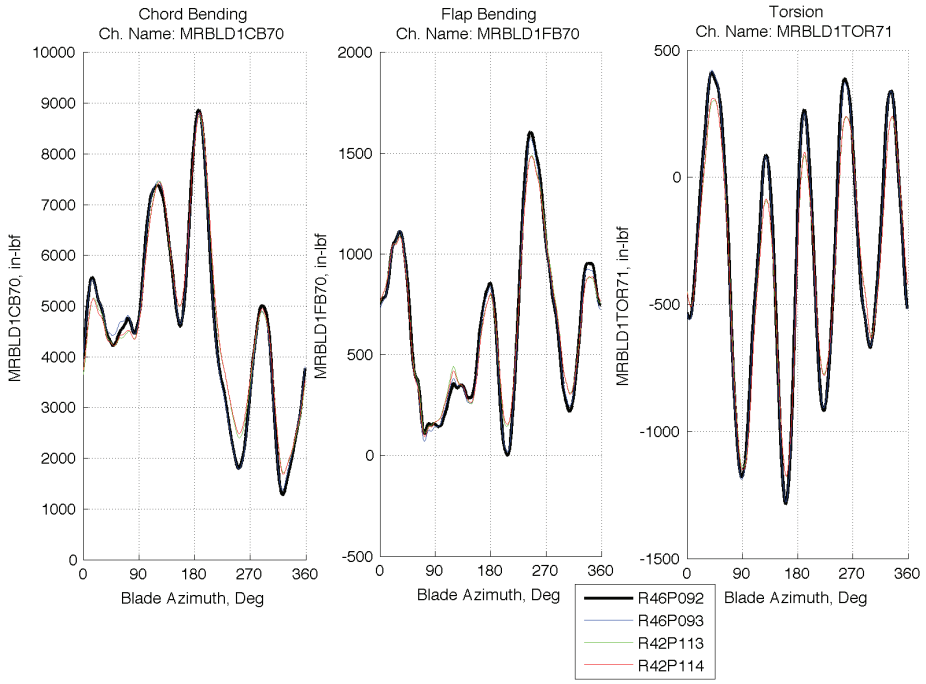

Figure D5. Blade chord- and flap-bending at station 70, and torsion at station 71.

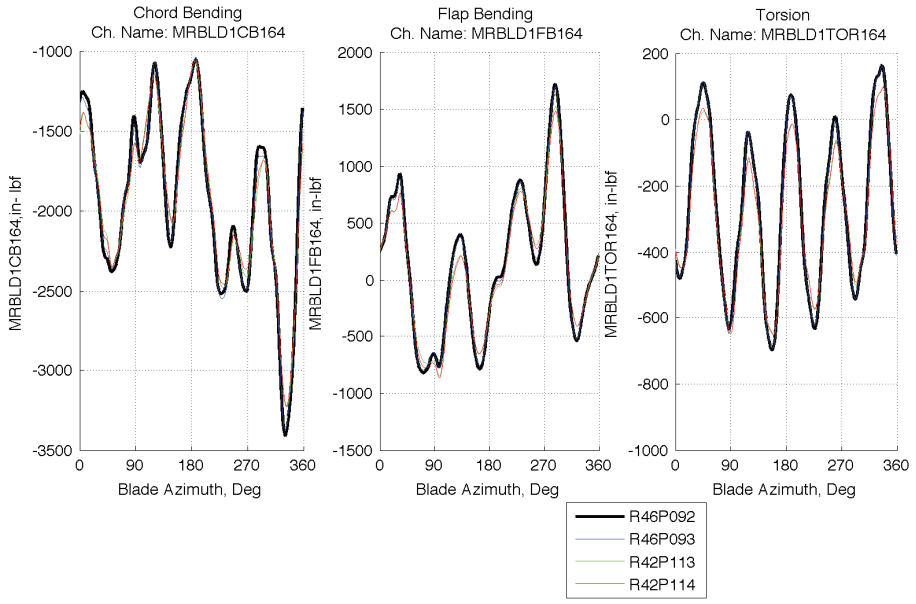

Figure D6. Blade chord-bending, flap-bending, and torsion at station 164.

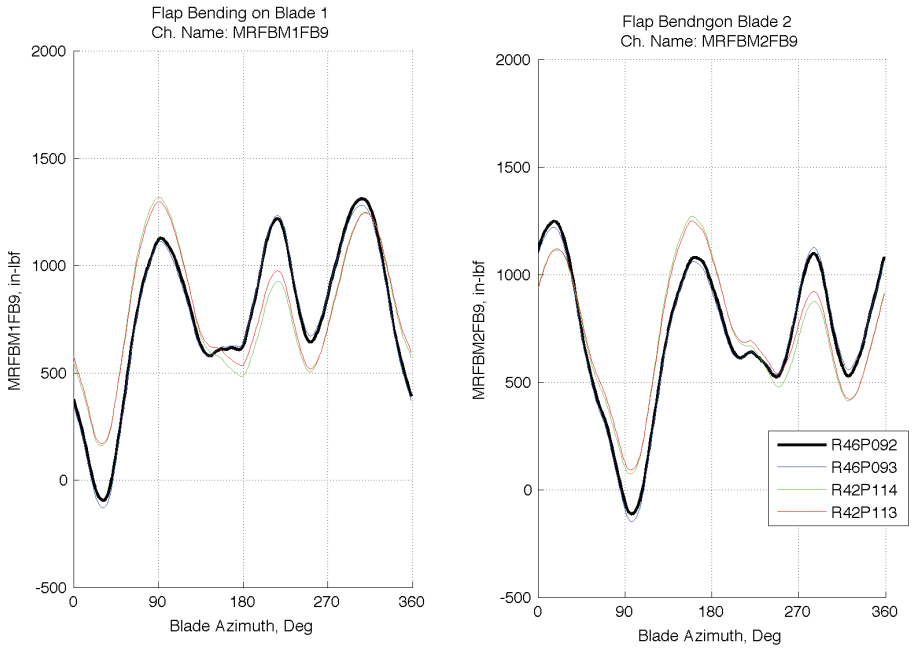

Figure D7. Flap-bending of flexbeam 1 and 2 at station 9.

The standard deviations, calculated from 64 revolutions of data at each azimuth, are also plotted for all channels to show the appropriate scatter-band for the SMART1 case, and compared with the averaged revolution and a revolution synthesized from the integer harmonics (figs. D8 to D14). The three in-plane acoustic channels and the rotor channels (drag, side, roll, and pitch) are band-pass filtered prior to plotting.

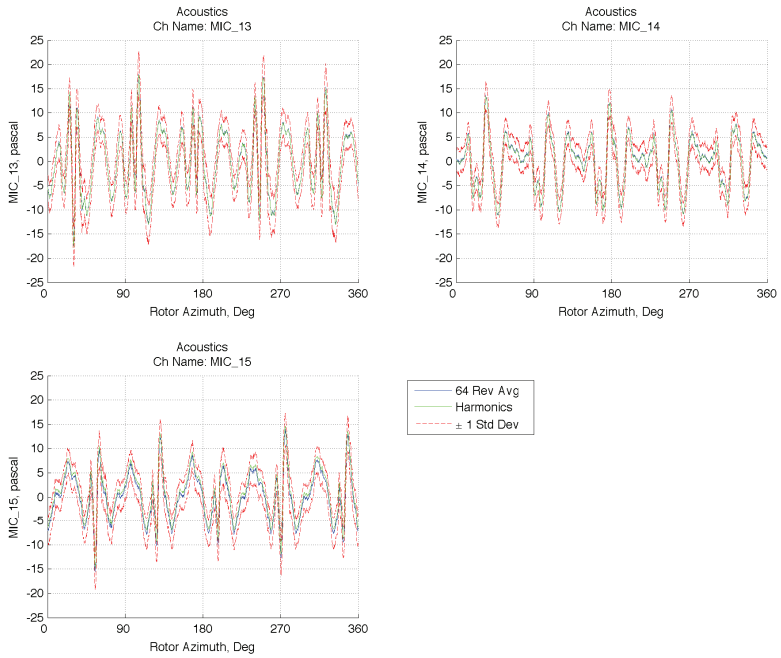

Figure D8. Standard deviation plots for acoustics.

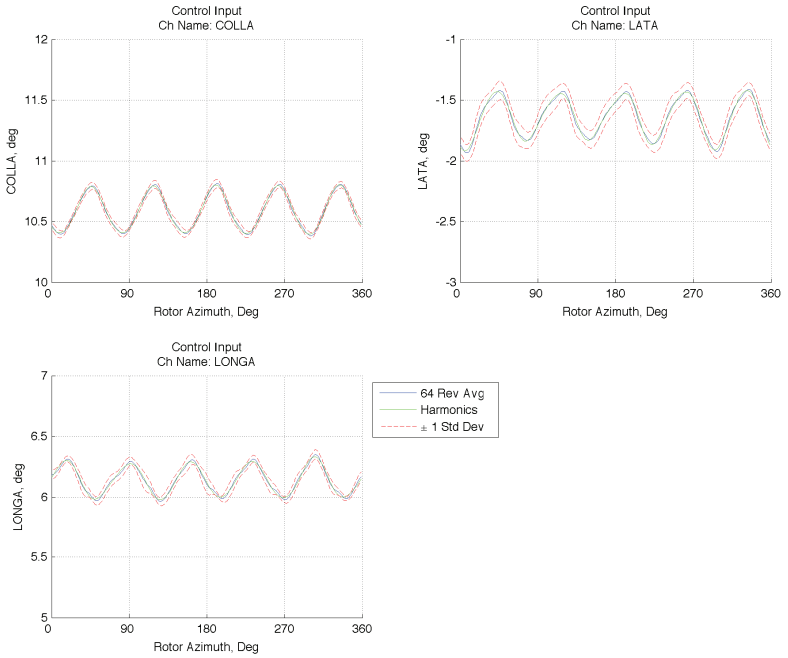

Figure D9. Standard deviation plots for control inputs.

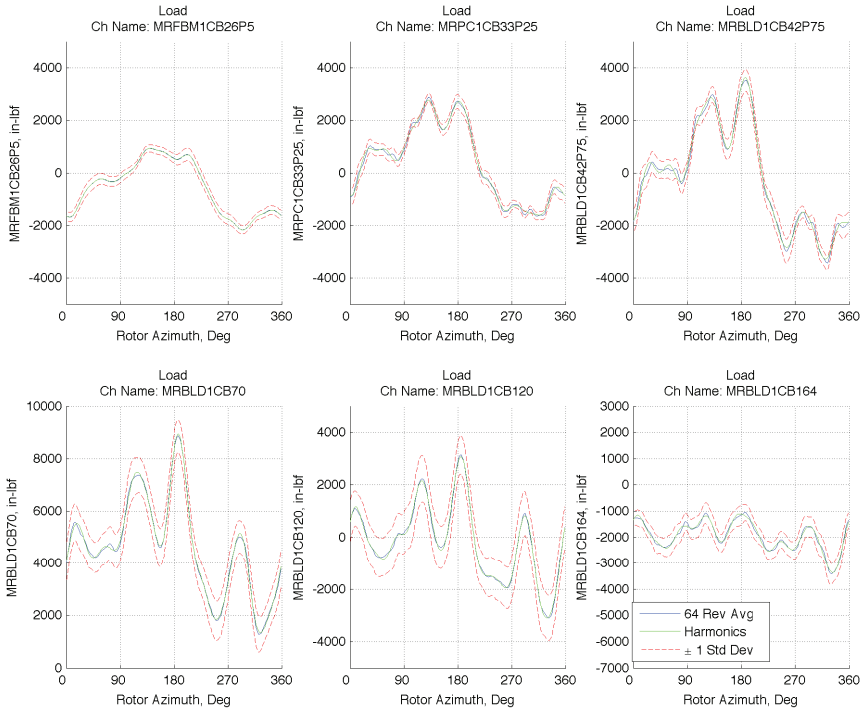

Figure D10. Standard deviation plots for chord-bending loads at various stations.

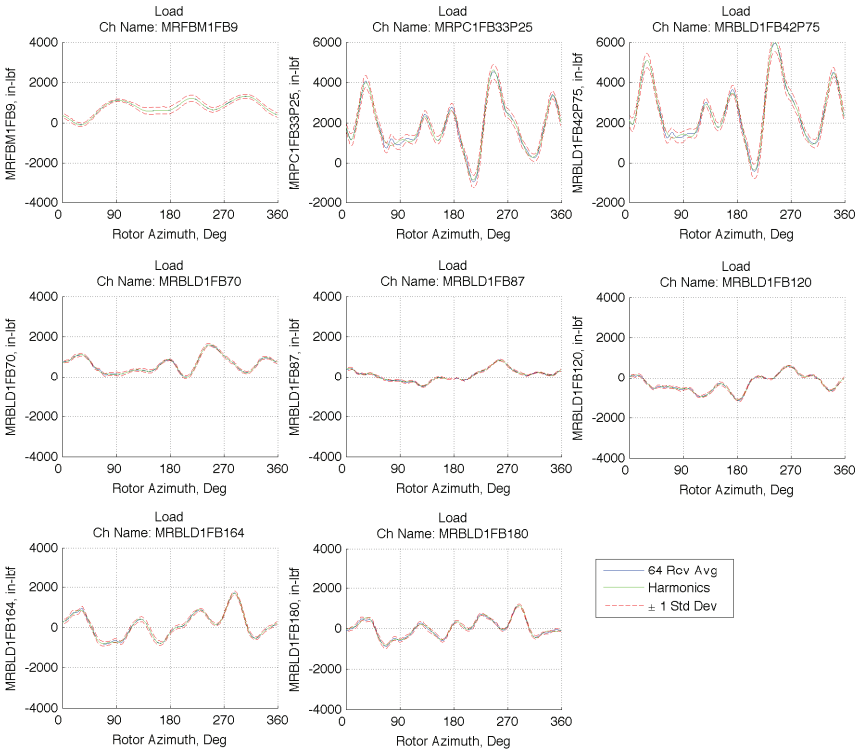

Figure D11. Standard deviation plots for flap-bending loads at various stations.

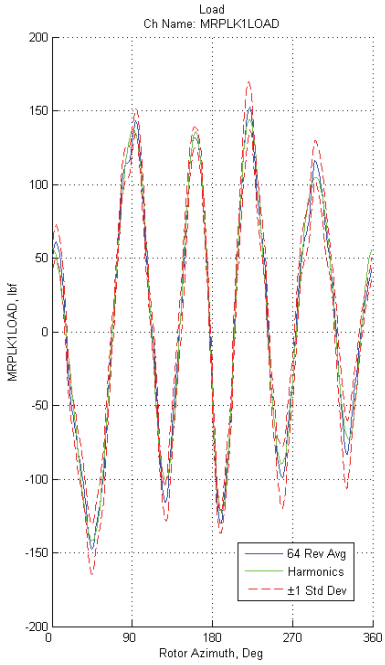

Figure D12. Standard deviation plot for pitch-link load.

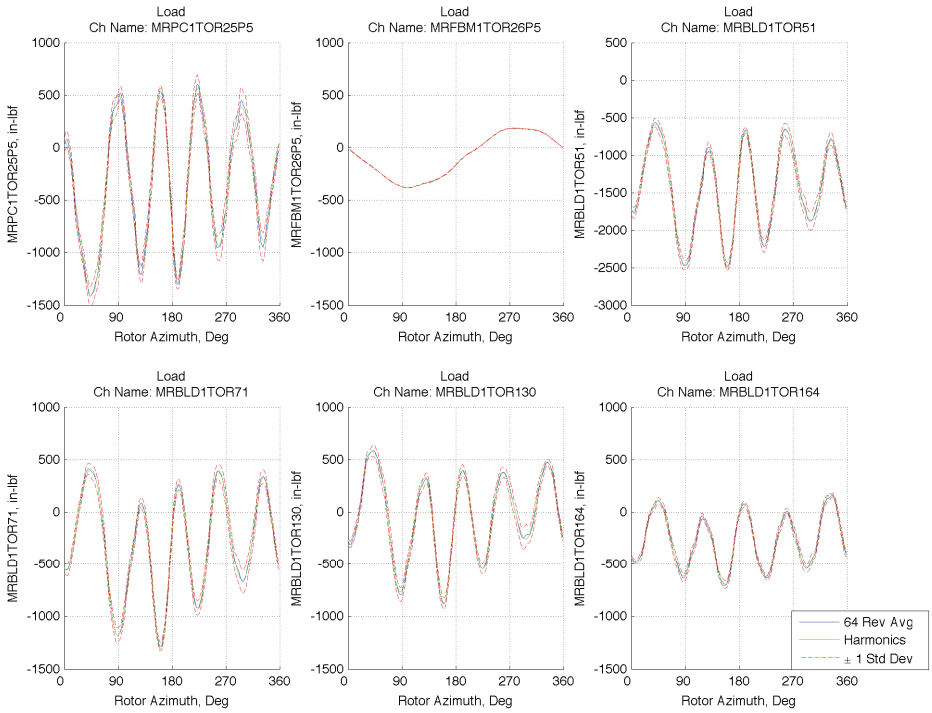

Figure D13. Standard deviation plots for torsion loads at various stations.

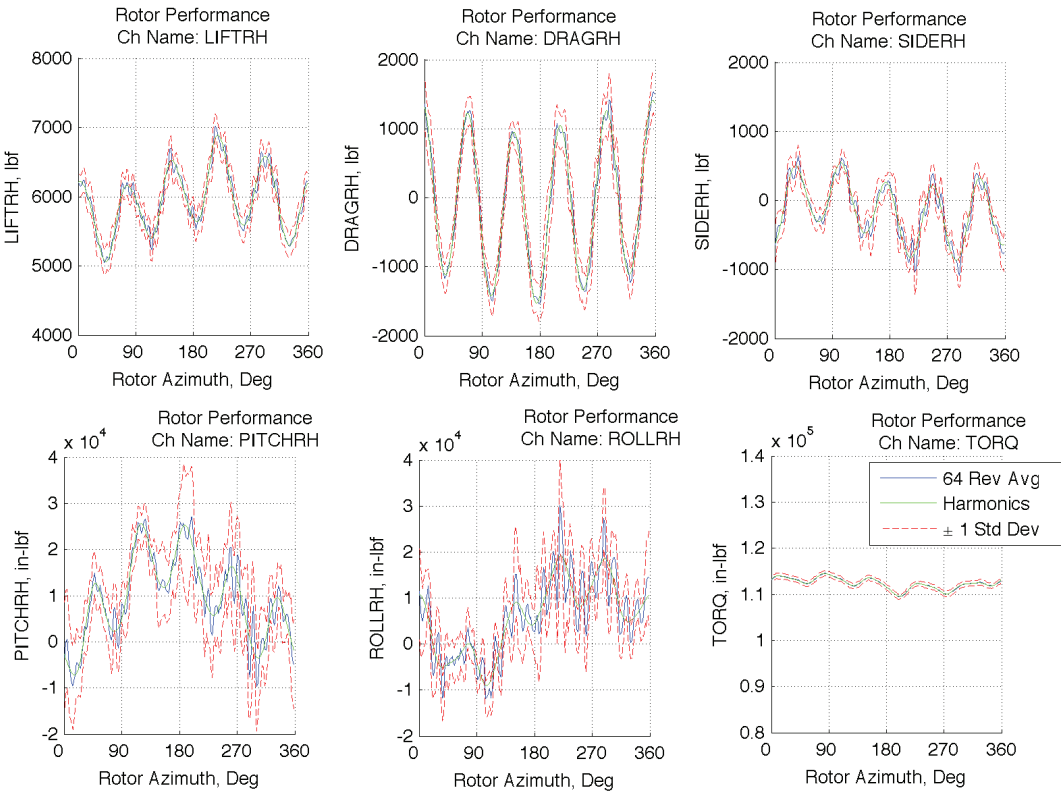

Figure D14. Standard deviation plots for rotor performance.

Appendix E
SMART2 Summary Plots

In Appendix E, repeatability for all three SMART2 test points (table 4) were plotted along with the HQP requirements to show data regularity. These plots (figs. E1 to E17) include flap schedules of all five flaps, acoustics for the three in-plane microphones, rotor performance at the rotor hub, and structural loading on blade #1. Unless indicated, the azimuth for all plots is referenced to the azimuthal angle of blade #1. The thick line in figures E1 to E7 corresponds to the representative data point selected.

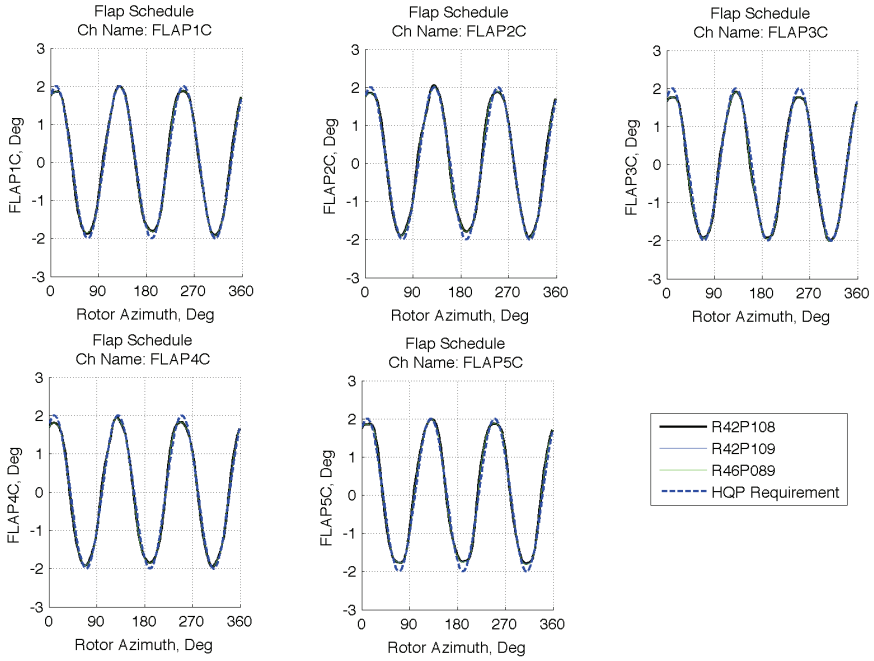

Figure E1. Comparison of measured active-flap schedule of blades #1 to #5 with HQP requirements, plotted against the local blade azimuth.

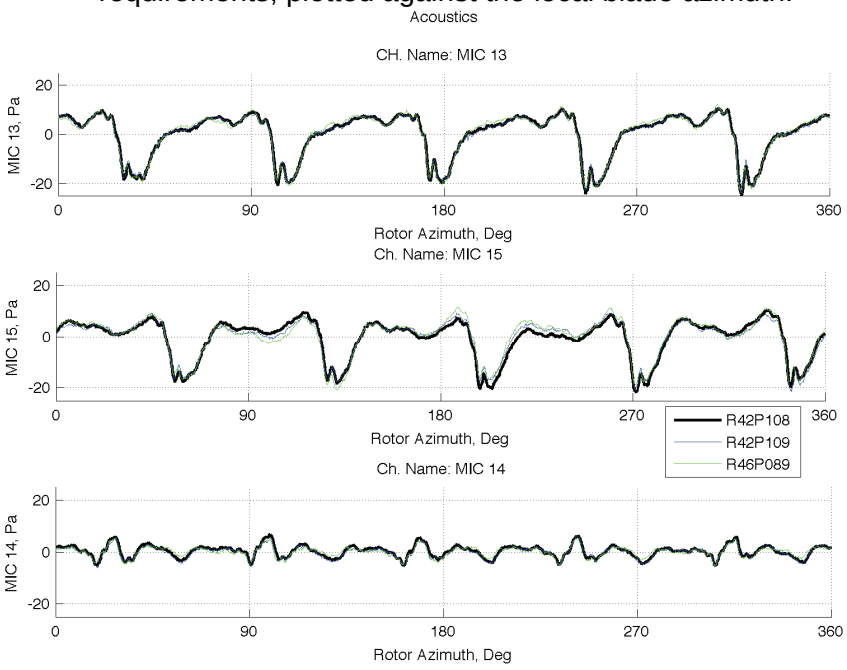

Figure E2. Microphones M13, M15, and M14.

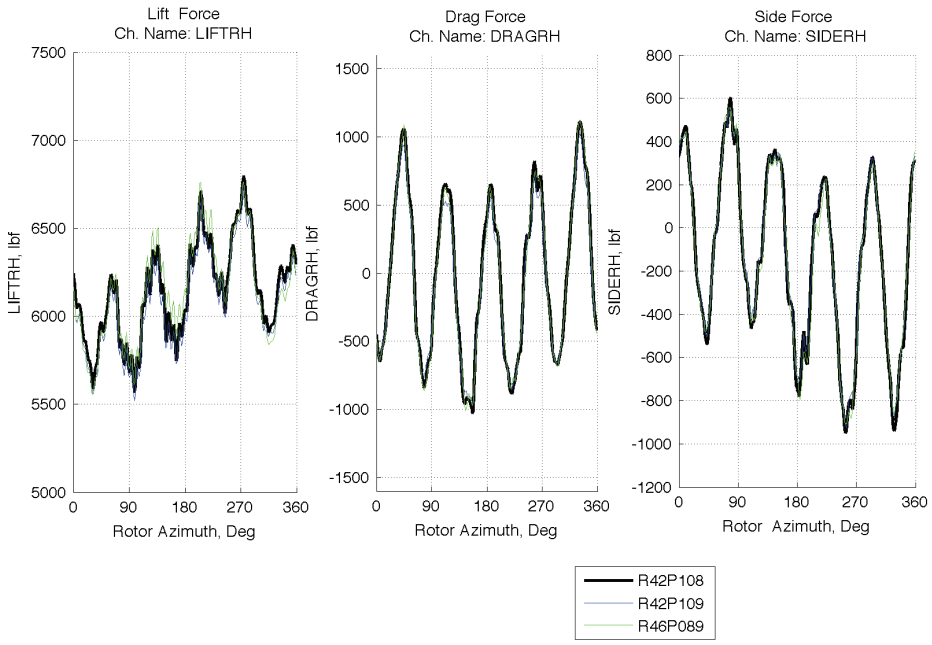

Figure E3. Lift, drag, and side forces at rotor hub.

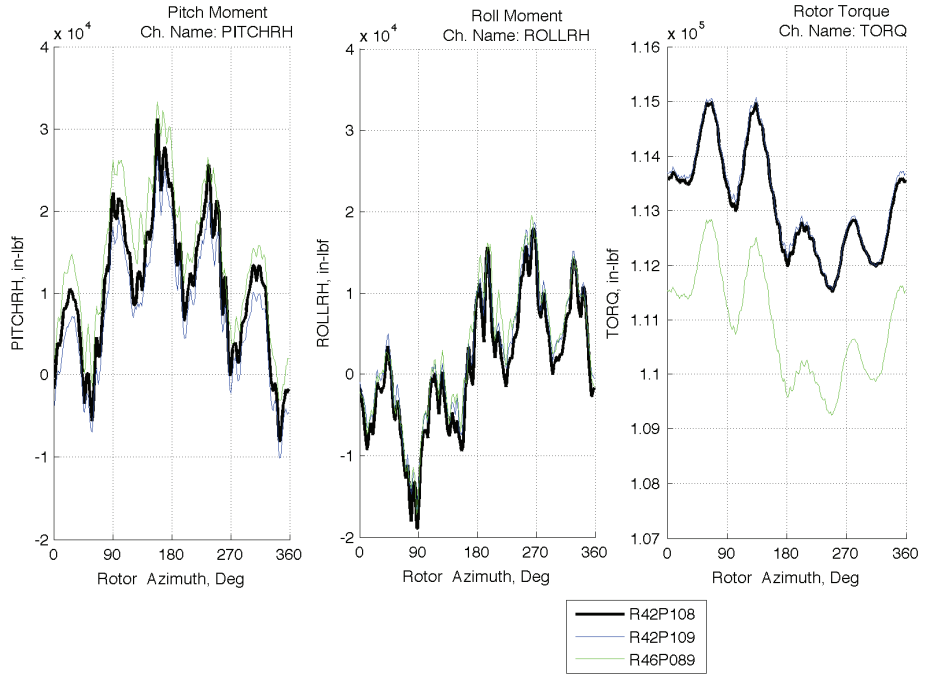

Figure E4. Pitching moment, rolling moment, and rotor torque at rotor hub.

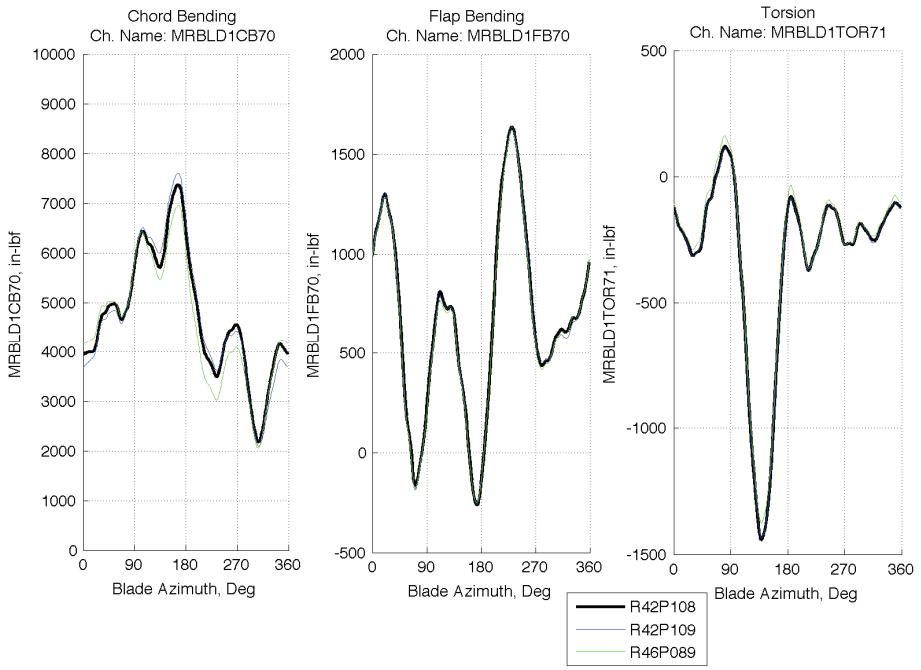

Figure E5. Blade chord- and flap-bending at station 70, and torsion at station 71.

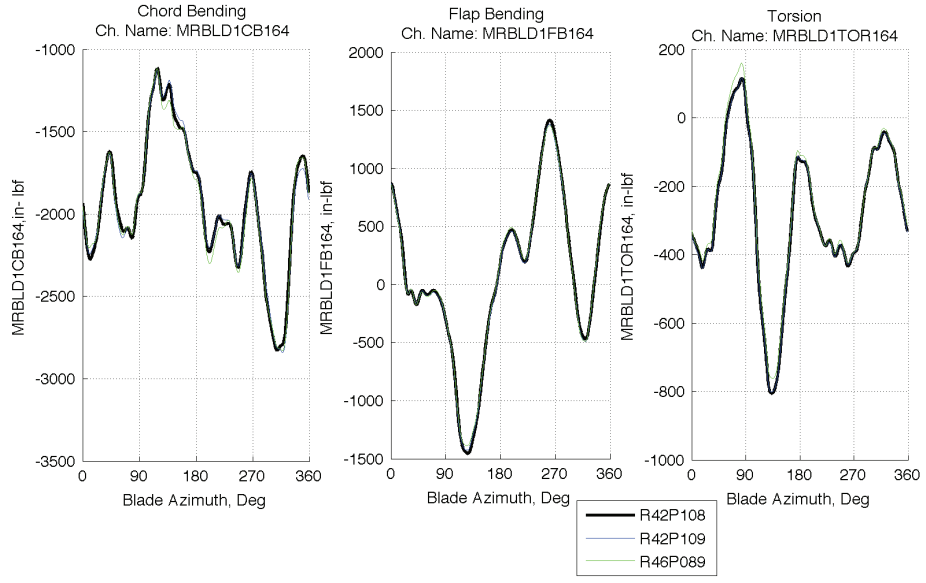

Figure E6. Blade chord-bending, flap-bending, and torsion at station 164.

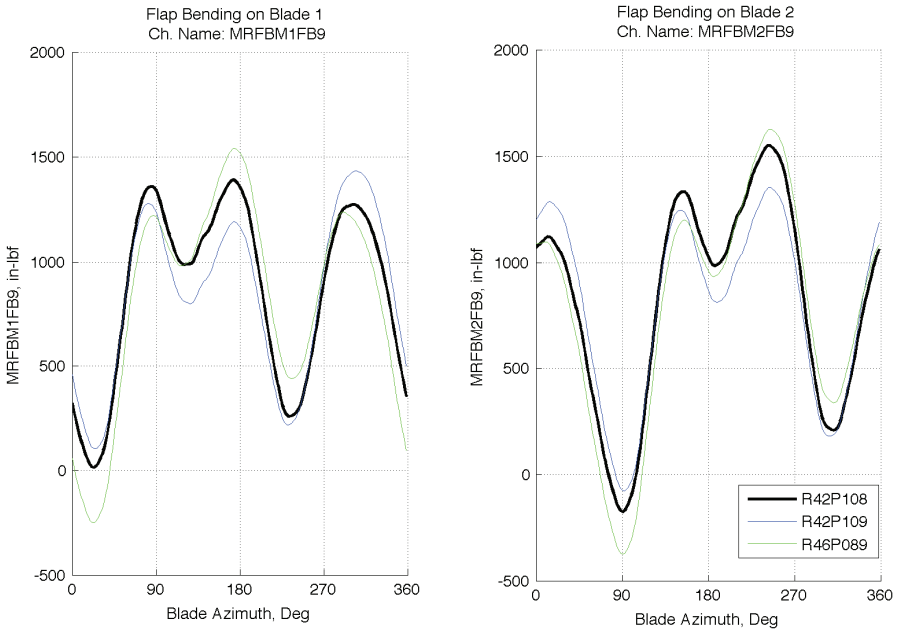

Figure E7. Flap bending of flexbeam 1 and 2 at station 9.

The standard deviations, calculated from 64 revolutions of data at each azimuth, are also plotted for all channels to show the appropriate scatter-band for the SMART2 case, and compared with the averaged revolution and a revolution synthesized from the integer harmonics (figs. E8 to E14). The three in-plane acoustic channels and the rotor channels (drag, side, roll, and pitch) are band-pass filtered prior to plotting.

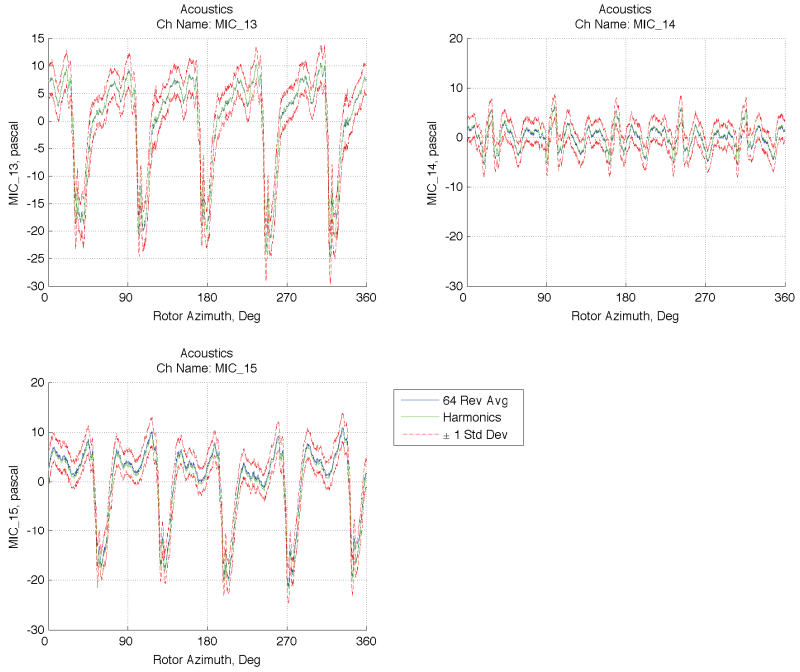

Figure E8. Standard deviation plots for acoustics.

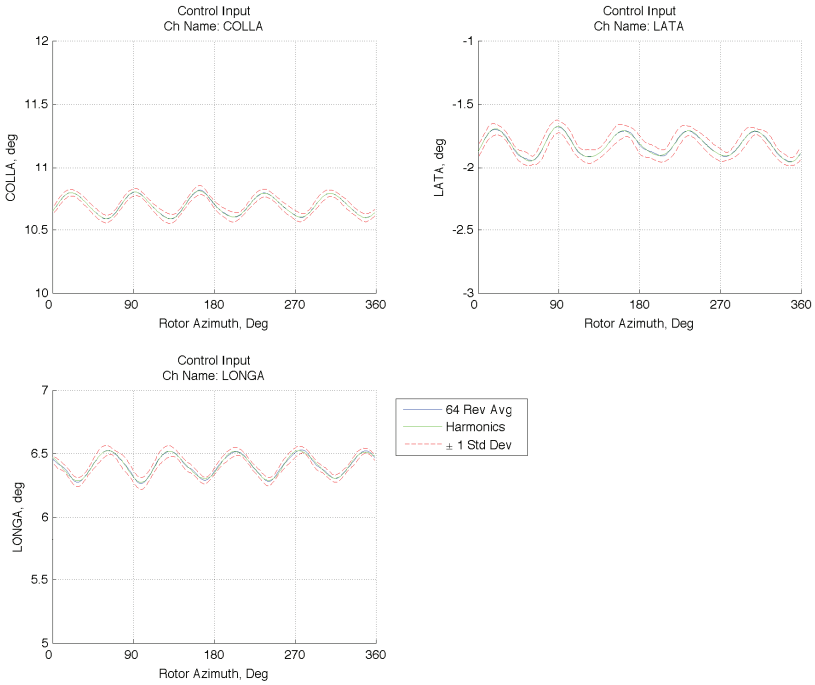

Figure E9. Standard deviation plots for control inputs.

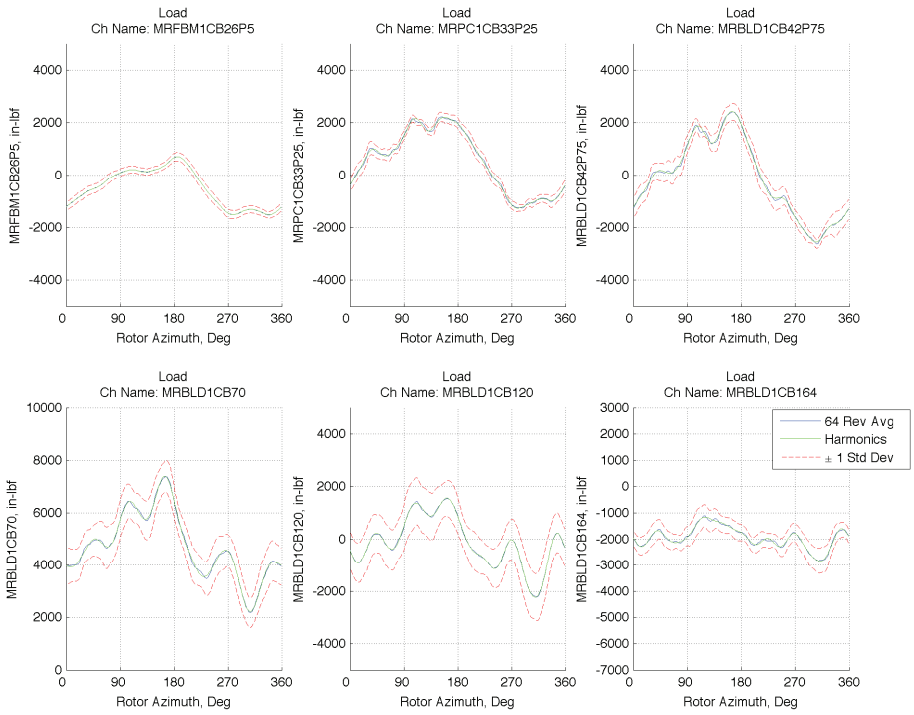

Figure E10. Standard deviation plots for chord-bending loads at various stations.

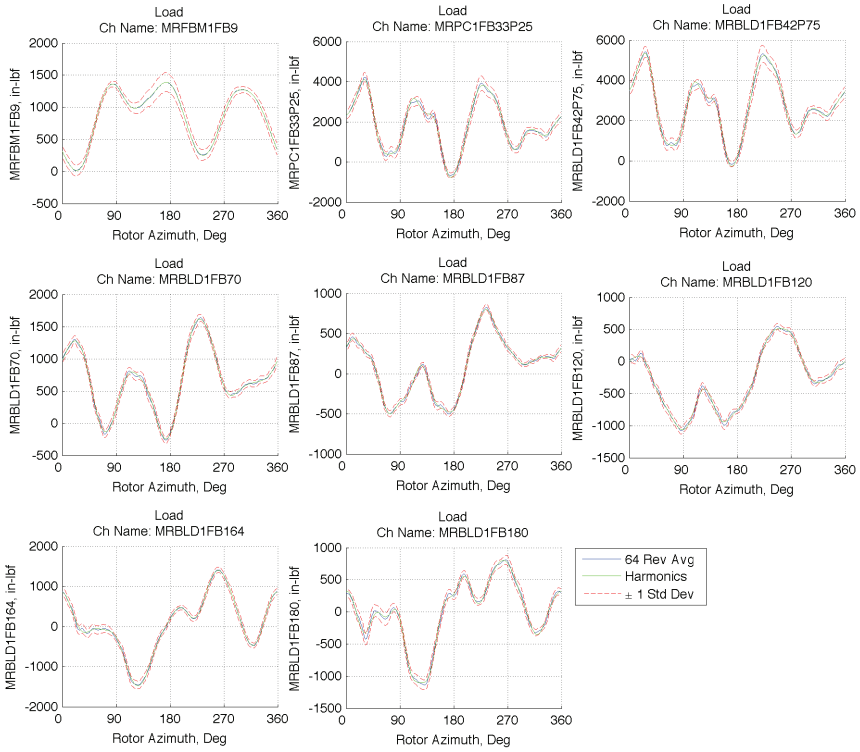

Figure E11. Standard deviation plots for flap-bending loads at various stations.

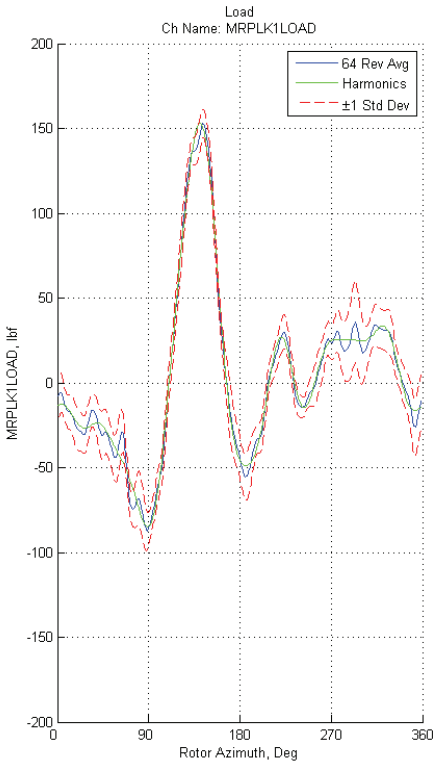

Figure E12. Standard deviation plot for pitch-link load.

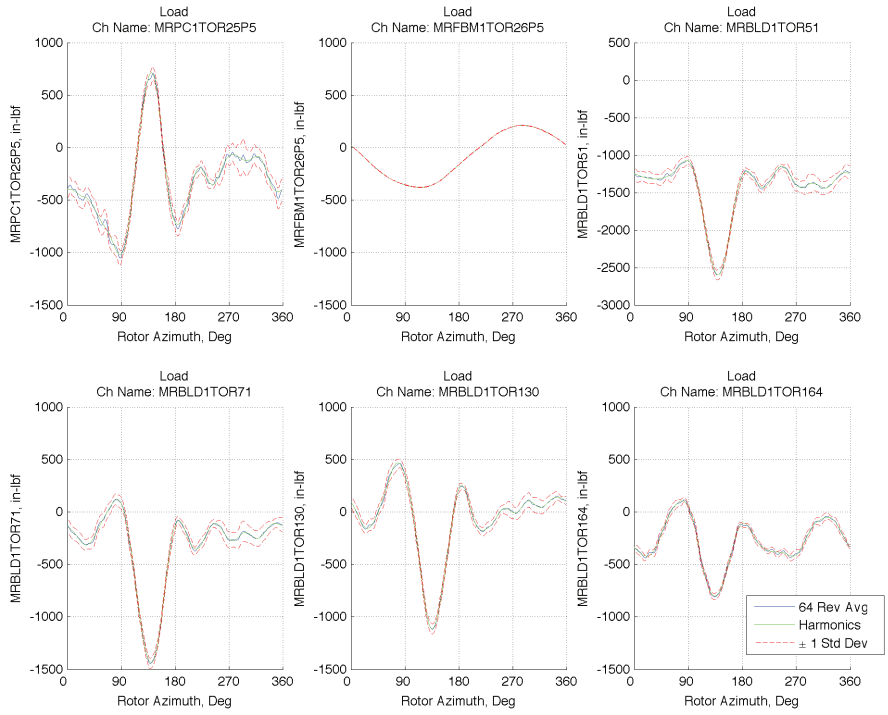

Figure E13. Standard deviation plots for torsion loads at various stations.

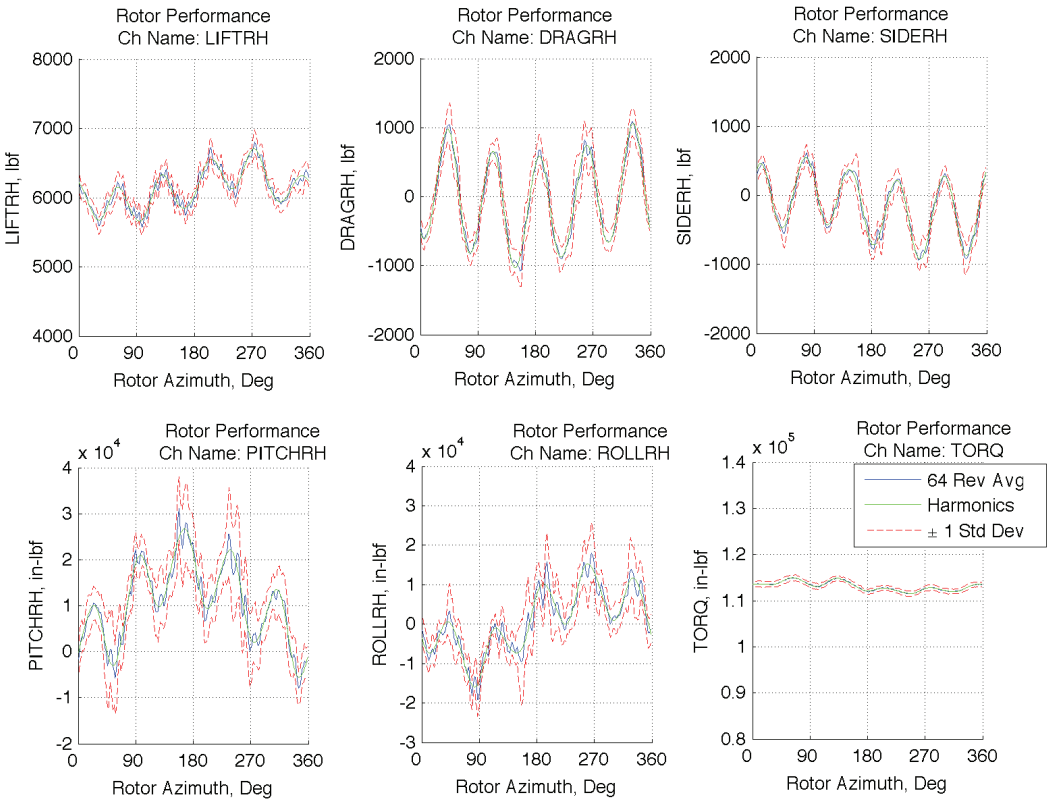

Figure E14. Standard deviation plots for rotor performance.

Appendix F

SMART4 Summary Plots

In Appendix F, repeatability for all six SMART4 test points (table 4) were plotted along with the HQP requirements to show data regularity. These plots include flap schedules of all five flaps, acoustics for the three in-plane microphones, rotor performance at the rotor hub, and structural loading on blade #1. Unless indicated, the azimuth for all plots is referenced to the azimuthal angle of blade #1. The thick line in figures F1 to F7 corresponds to the representative data point selected.

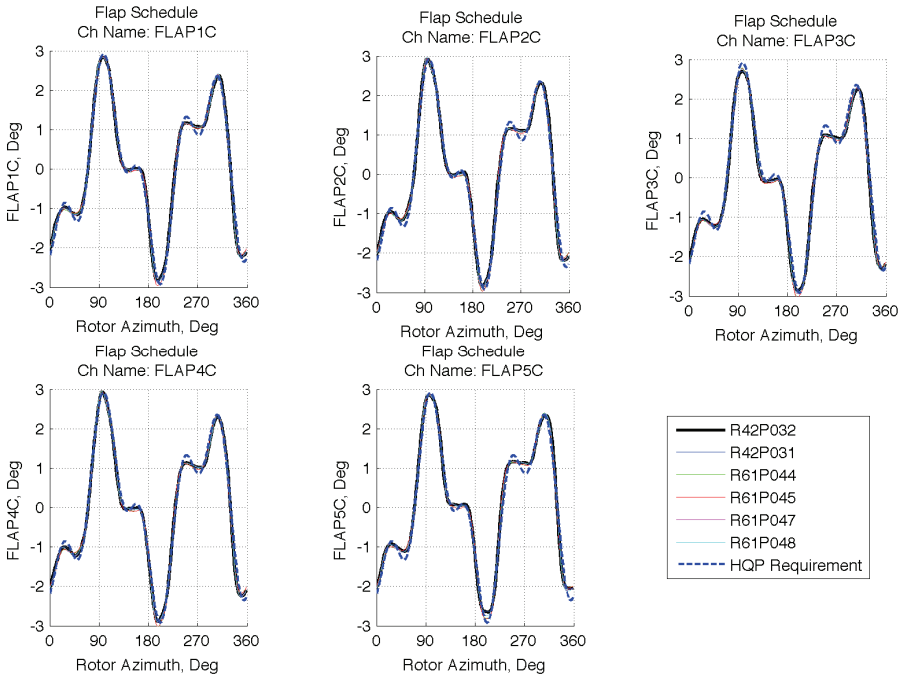

Figure F1. Comparison of measured active-flap schedule of blades #1 to #5 with HQP requirements, plotted against the local blade azimuth.

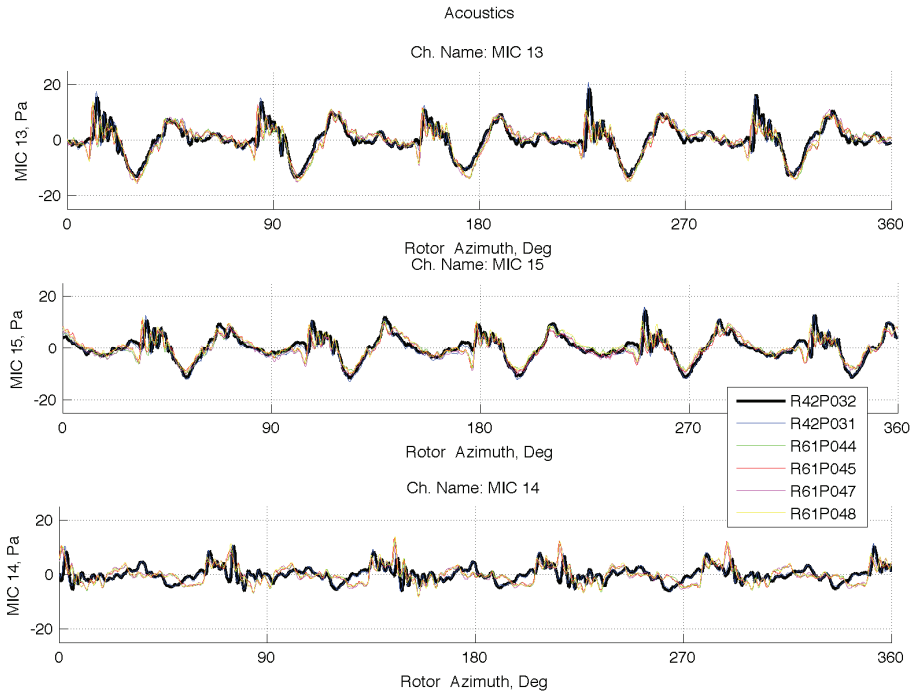

Figure F2. Microphones M13, M15, and M14.

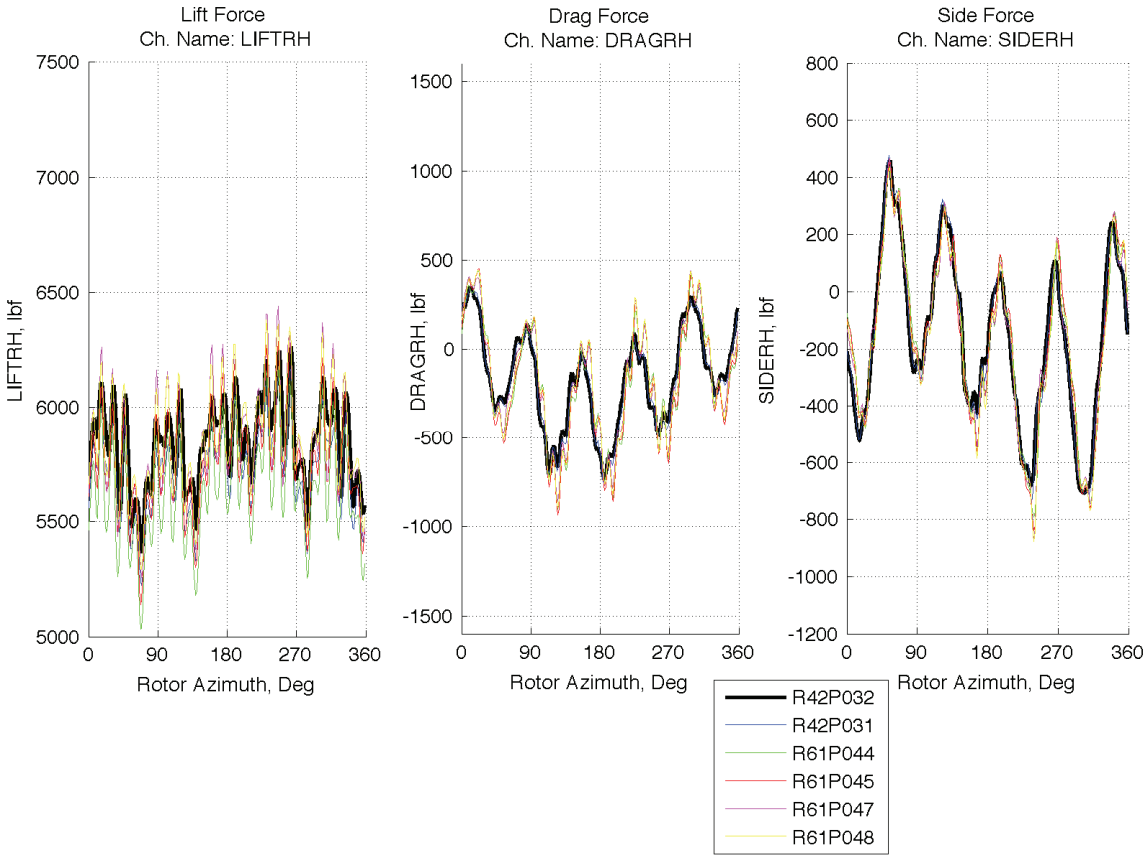

Figure F3. Lift, drag, and side forces at rotor hub.

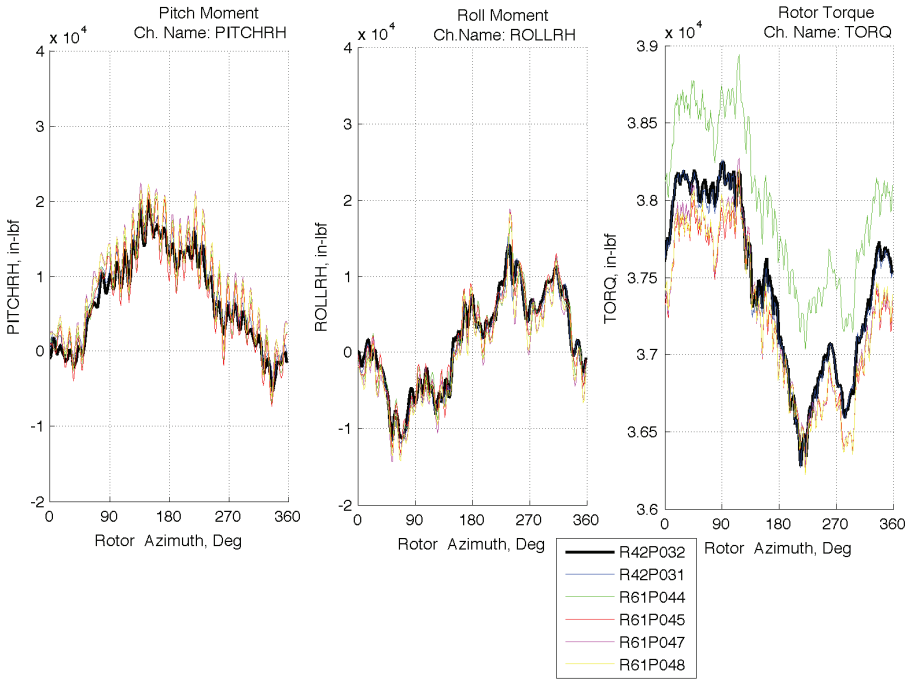

Figure F4. Pitching moment, rolling moment, and rotor torque at rotor hub.

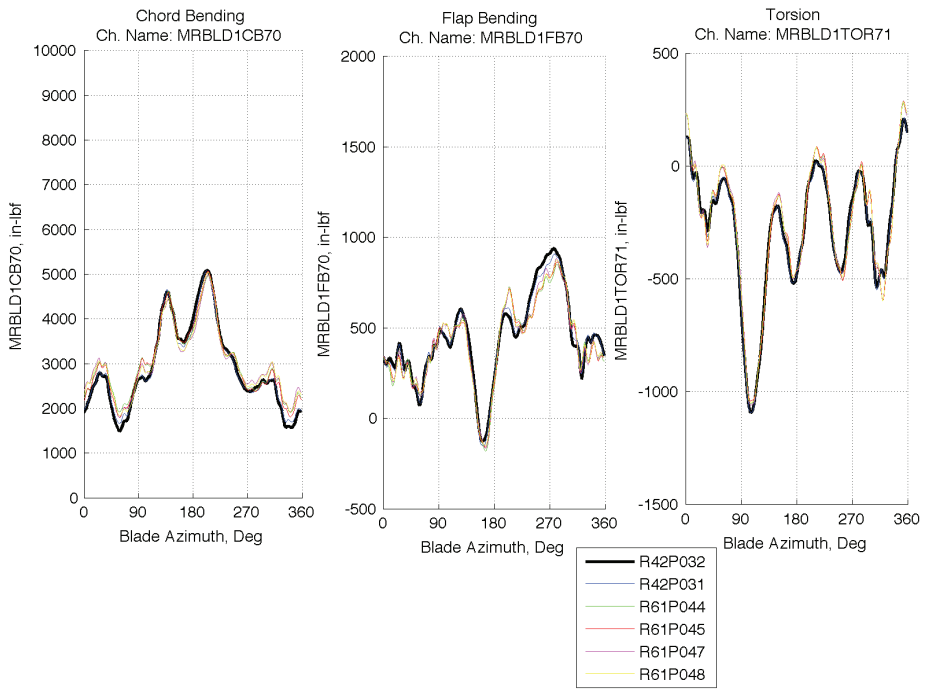

Figure F5. Blade chord- and flap-bending at station 70, and torsion at station 71.

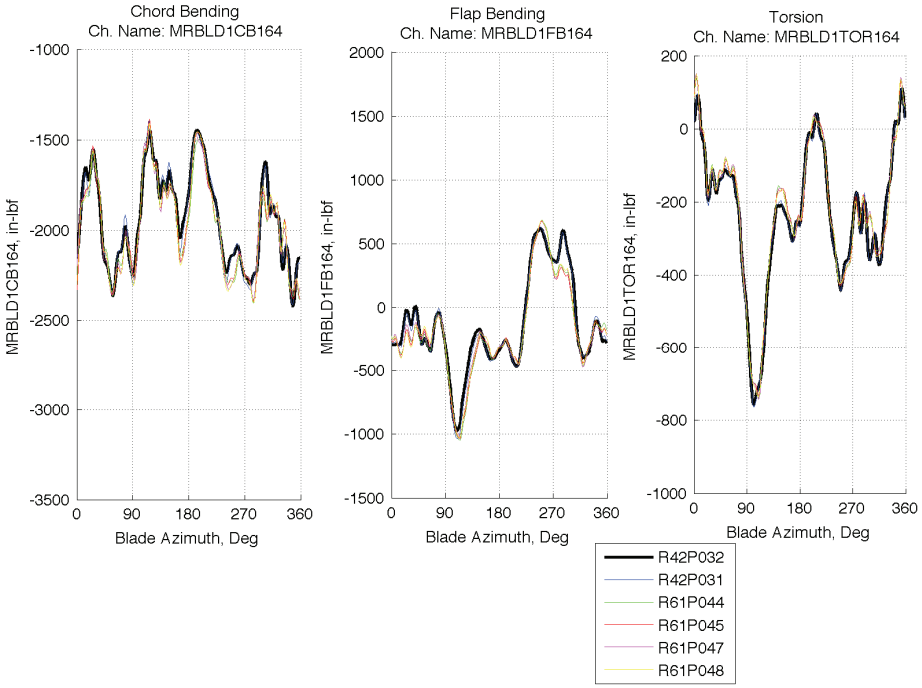

Figure F6. Blade chord-bending, flap-bending, and torsion at station 164.

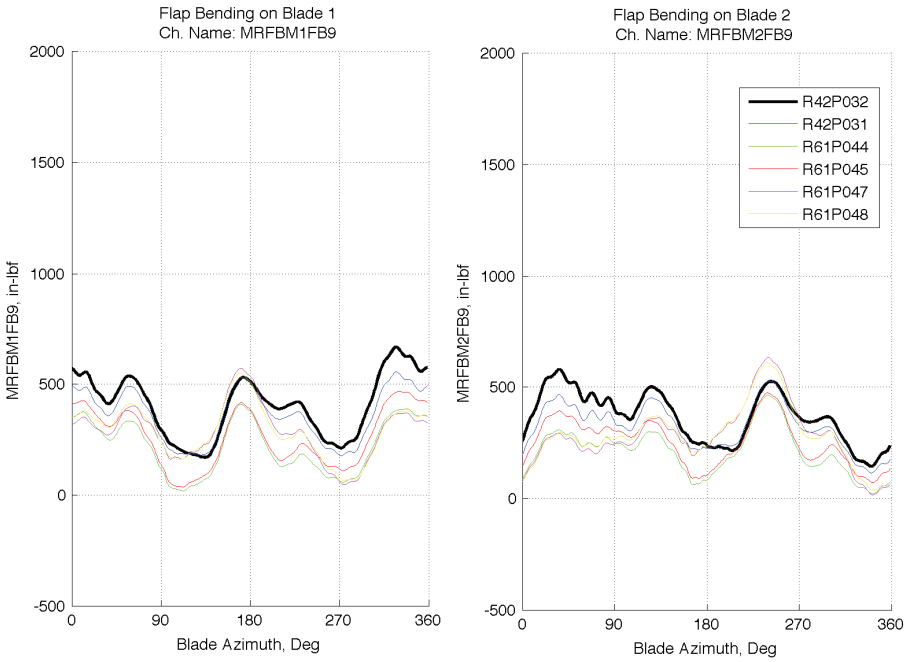

Figure F7. Flap bending of flexbeam 1 and 2 at station 9.

The standard deviations, calculated from 64 revolutions of data at each azimuth, are also plotted for all channels to show the appropriate scatter-band for the SMART4 case, and compared with the averaged revolution and a revolution synthesized from the integer harmonics (figs. F8 to F14). The three in-plane acoustic channels and the rotor channels (drag, side, roll, and pitch) are band-pass filtered prior to plotting.

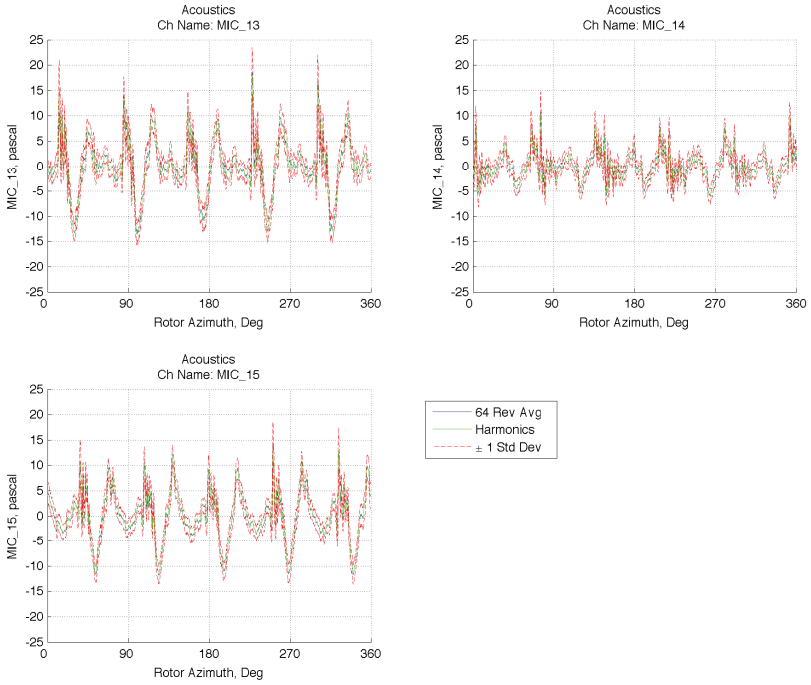

Figure F8. Standard deviation plots for acoustics.

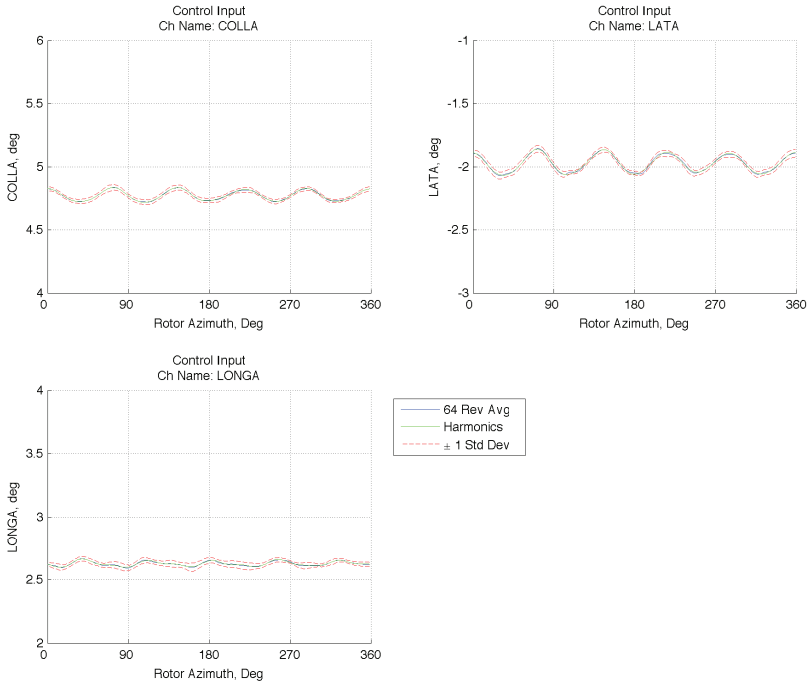

Figure F9. Standard deviation plots for control inputs.

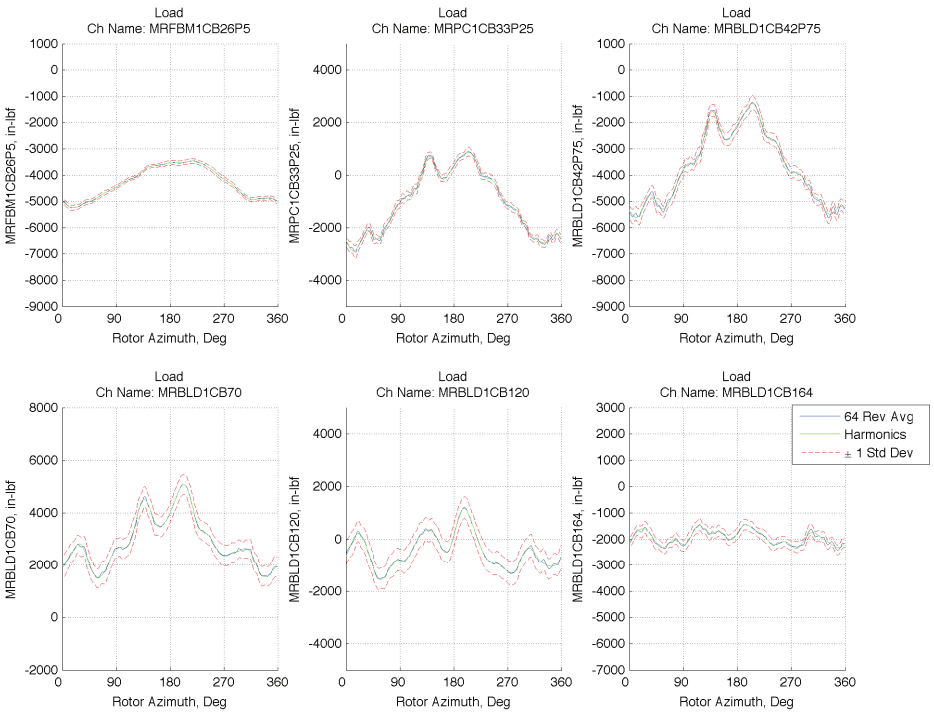

Figure F10. Standard deviation plots for chord-bending loads at various stations.

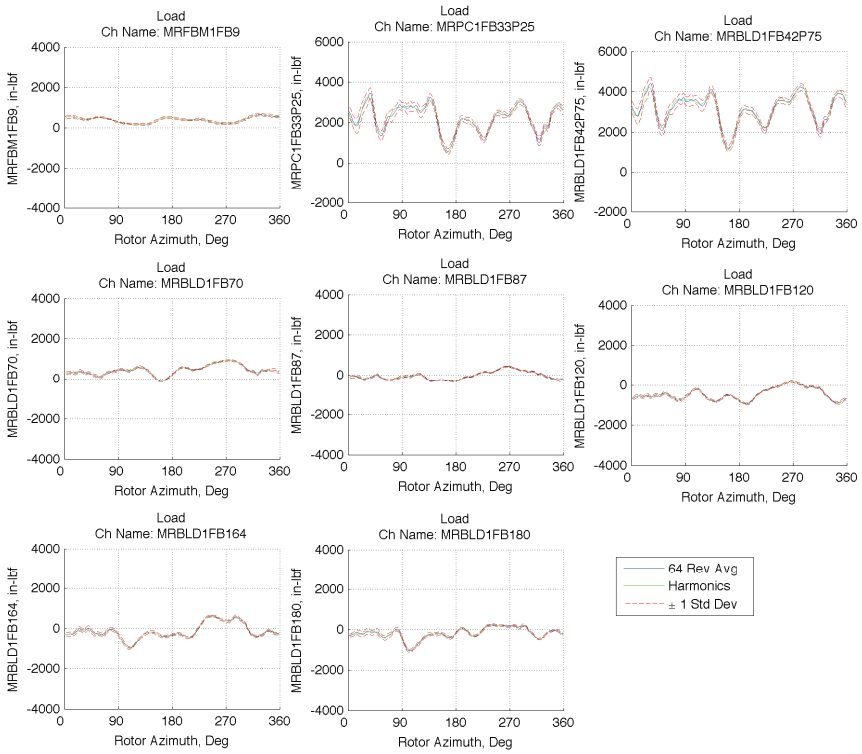

Figure F11. Standard deviation plots for flap-bending loads at various stations.

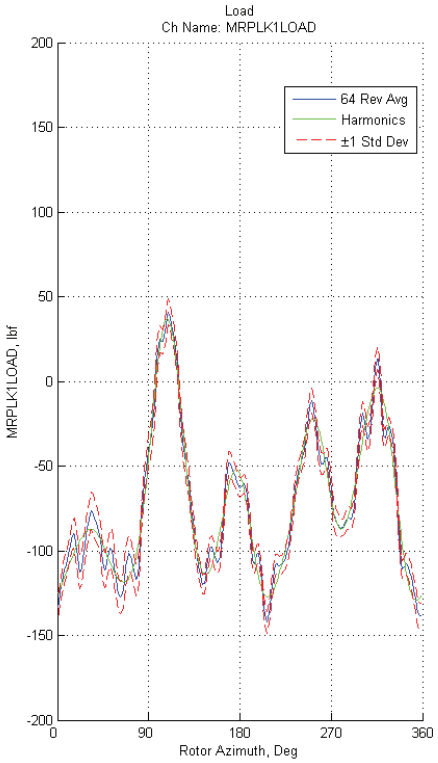

Figure F12. Standard deviation plot for pitch-link load.

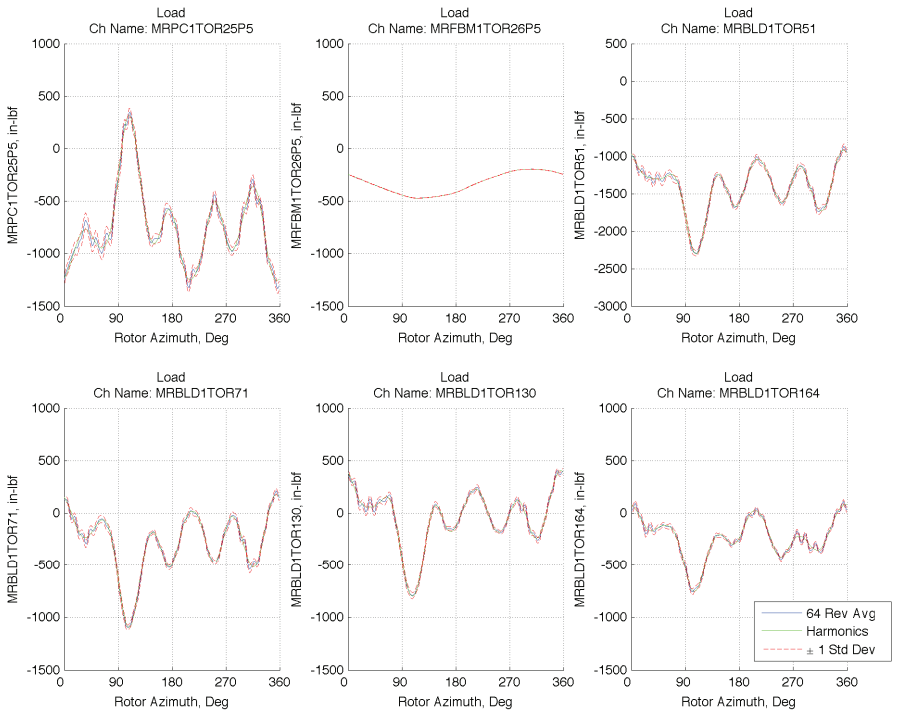

Figure F13. Standard deviation plots for torsion loads at various stations.

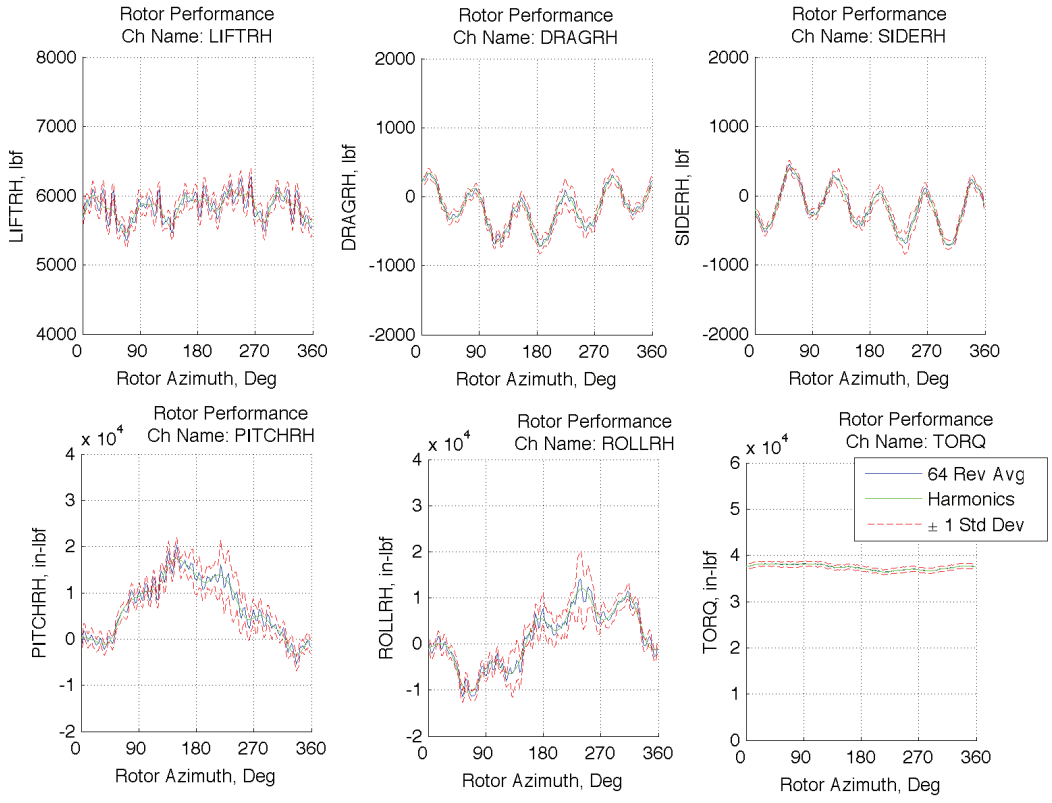

Figure F14. Standard deviation plots for rotor performance.

Appendix G

CD Contents

Appendix G describes the contents of the data CD enclosed with this report. It includes a description of the folder structure and the file hierarchy of all data presented. A copy of the HQP Phase Ib reporting guideline document (ref. 3) is also included, as well as an electronic copy of this report. An electronic copy of the contents in the data CD can also be obtained from Dr. William Warmbrodt (william.warmbrodt@nasa.gov, 650-604-5642), or Dr. Ben W. Sim (ben.w.sim@us.army.mil, 650-604-0608).

Data CD File Structure

The top-most level of the CD contains the follow files/folders:

- **`EXP_DATA`** (folder): This folder contains numerical data of all the channels as requested by DARPA for all five HQP Phase Ib test conditions.
- **`Phase1B_MileStone_Reporting_Guidlines.pdf`** (PDF document): A document, originally given to the HQP participants, that describes the format of the submitted data.
- **`Nasa TM-2010-216404 HQP_PhaseIb_DataReport.pdf`** (PDF document): An electronic copy of the current report.

EXP_DATA Folder

This folder contains the sensor/channel data acquired during the Boeing-SMART test for the specified HQP Phase Ib (table 1). All data files with `.dat` extension are stored in TAB-delimited, ASCII text format with `<LF>` as line break. The hierarchy of these stored data-files follows the format as specified by DARPA (ref. 3). All channel units can be found in Appendix A.

The contents of this folder are categorized by the five HQP Phase Ib test conditions. For each test condition, all associated experimental data are placed in a separate folder, with the file hierarchy shown below:

- EXP_DATA/
  - AUX_INFO/
    - README.TXT
    - Flight_summary.dat
    - EXP_DATA_STDEV/
    - MDART_AUX/
      - RxxPyyyHA.txt
      - RxxPyyyHCI.txt
      - RxxPyyyHL.txt
      - RxxPyyyHRP.txt
    - SMART1_AUX/
      - [*Same file structure as MDART_AUX/*]
    - SMART2_AUX/
      - [*Same file structure as MDART_AUX/*]
    - SMART3_AUX/
      - [*Empty*]

    - SMART4_AUX/
        - [*Same file structure as MDART_AUX/*]
- MDART/
    - Flight_condition.dat
    - EXP_2008/
        - Rotor_Performance/
        - Control_Inputs/
        - Cn_Cc_Cm/
        - LOAD_DATA/
        - ACOUSTIC/
- SMART_1/
    - [Same file structure as in SMART1/]
- SMART_2/
    - [*Same file structure as in SMART1/*]
- SMART_3/
    - [*Empty/*]
- SMART_4/
    - [*Same file structure as in SMART1/*]

For each test condition, the bulk of the data is stored within a folder named "EXP_2008/" and is sub-categorized into major measurement groups (e.g. Rotor_Performance/, Control_Inputs/, etc.). Detailed descriptions and data formats of these groups are reported in reference 3 and will not be repeated here. Following the requirements outlined in reference 3, a Flight_condition.dat file is also included that summarizes the (measured) operating conditions of the rotor for each HQP Phase Ib test condition with additional flight parameters pending at the end.

Some important notes regarding the content of this folder are noted below:

- Due to the lack of surface pressure measurement in the Boeing-SMART rotor test, there are no airload and airfoil pitching moment data available. The contents within the "Cn_Cc_Cm/" folder are left blank.
- Tare data are not reported in the "LOAD_DATA/" folder as all reported pitch link and blade structural load channels already had zero-tare correction.
- There are no data reported for the high-speed SMART3 condition (table 1) as the test point could not be acquired due to high flex-beam and load limits. No data files were inserted under the "SMART_3/" folder.

AUX_INFO Folder

The AUX_INFO folder contains auxiliary data pertaining to the test. The README.TXT file describes the folders and their contents. The Flight_summary.dat file combines the Flight_condition.dat files from all four test cases into one file for ease of comparison. Inside the AUX_INFO folder, there are EXP_DATA_STDEV folder and a *case*_AUX folder for each of the four test cases.

*case*_AUX Folder

The *case*_AUX folder contains the cosine-sine harmonic pairs for all channels. For acoustic channels, the integer harmonics from 0 to 511 are saved in the file RxxPyyyHA.txt. All other channels have integer harmonics from 0 to 10 and are saved in RxxPyyyHCI.txt for control-inputs, RxxPyyyHL.txt for structural loads, and RxxPyyyHRP.txt for rotor performance, where xx and yy are the run and the point numbers, respectively. Again no data is available in the "SMART3_AUX/" folder.

EXP_DATA_STDEV Folder

The standard deviations of each measurement channel, shown in Appendices G to J, are stored in this directory. Each HQP Phase Ib test condition comes with two data files: one for acoustics channels (*case*_STDEV_ACOUSTIC.dat) alone and another (*case*_STDEV_ROTOR.dat) for all other channels listed in Appendix A.

- EXP_DATA_STDEV/
  - MDART_STDEV_ACOUSTIC.dat (figure C7)
  - MDART_STDEV_ROTOR.dat (figure C8 to C14)
  - SMART1_STDEV_ACOUSTIC.dat (figure D7)
  - SMART1_STDEV_ROTOR.dat (figure D8 to D14)
  - SMART2_STDEV_ACOUSTIC.dat (figure E7)
  - SMART2_STDEV_ROTOR.dat (figure E8 to E14)
  - SMART3_STDEV_ACOUSTIC.dat (figure F7)
  - SMART3_STDEV_ROTOR.dat (figure F8 to F14)

The standard deviations are derived from evaluating data scatter associated with 64-revolutions of time-history data. Standard-deviation data for all three in-plane microphone channels (M13, M14 and M15) are stored in the *case*_STDEV_ACOUSTIC.dat. The first column contains data pertaining to the scan index (ranging from 1 to 2048) that depicts the 2048 azimuthal positions recorded during one rotor revolution. The remaining three columns represent the standard deviations for channels M13, M14 and M15 respectively. The standard deviations for the rest of the performance, controls, and blade structural load channels are stored in file *case*_STDEV_ROTOR.dat in a similar manner. Each channel (column) contains information corresponding to 256 recorded azimuth positions for each rotor revolution. The conversion from scan index to rotor azimuth (deg.) can be calculated out as followed: $\psi_k=(360^\circ/N)\cdot(scan\_index\ -1)$, where N is 2048 for acoustics, or 256 for all other sensors/channels. Note that there are no data for the SMART3 test condition due to reasons as discussed before.